Closed-loop optogenetic perturbation of macaque oculomotor cerebellum: evidence for an internal saccade model

Abbreviated title: Perturbation of cerebellar internal model

Robijanto Soetedjo[1,2] and Gregory D. Horwitz[1,2]

[1]Department of Physiology and Biophysics, University of Washington, Seattle, WA 98195, USA

[2]Washington National Primate Research Center, University of Washington, Seattle, WA 98195, USA.

Corresponding author:

Robijanto Soetedjo,

Department of Physiology and Biophysics, Box 357290,

University of Washington, Seattle, WA 98195

Email: robi@uw.edu

Number of pages: 41

Number of figures: 13

Number of tables: 2

Number of words for abstract: 219

Number of words for introduction: 571

Number of words for discussion: 1500

Acknowledgments: National Institute of Health fundings: EY028902 (RS), EY030441 (GH), OD010425, RR00166 (Washington National Primate Research Center), P30EY001730 (Vision Research Core of University of Washington). The authors thank Dr. Albert Fuchs for his valuable comments and editorial assistance.

The authors declare no competing financial interests.

Abstract

Internal models are essential for the production of accurate movements. The accuracy of saccadic eye movements is thought to be mediated by an internal model of oculomotor mechanics encoded in the cerebellum. The cerebellum may also be part of a feedback loop that predicts the displacement of the eye and compares it to the desired displacement in real time to ensure that saccades land on target. To investigate the role of the cerebellum in these two aspects of saccade production, we delivered saccade-triggered light pulses to channelrhodopsin-2-expressing Purkinje cells in the oculomotor vermis (OMV) of two macaque monkeys. Light pulses delivered during the acceleration phase of ipsiversive saccades slowed the deceleration phase. The long latency of these effects, and their scaling with light pulse duration, are consistent with an integration of neural signals downstream of the stimulation. In contrast, light pulses delivered during contraversive saccades reduced saccade velocity at a short latency (~6 ms) that was followed by a compensatory reacceleration which caused gaze to land near or on the target. We conclude that the contribution of the OMV to saccade production depends on saccade direction; the ipsilateral OMV is part of a forward model that predicts eye displacement, whereas the contralateral OMV is part of an inverse model that creates the force required to move the eyes accurately.

Significance Statement

Theory and experiment suggest that saccade production involves an internal model of oculomotor mechanics that resides inside the cerebellum. How cerebellar neurons implement this model is poorly understood. To illuminate this issue, we stimulated Purkinje cells in the oculomotor vermis (OMV) optogenetically during saccades and examined the resultant movement deviations. Stimulation of the contralateral OMV affected saccade dynamics at short latency, suggesting that the contralateral OMV is part of the feedforward circuit that produces the saccade motor command. In contrast, perturbation of the ipsilateral OMV affected saccade dynamics at a longer latency; it prolonged the saccade deceleration phase, leading to hypermetria. This dysmetria is consistent with perturbation of the eye displacement integrator in the feedback loop of the saccade generator.

Introduction

The generation of accurate saccades requires an intact cerebellum (Takagi et al., 1998; Barash et al., 1999). Purkinje (P-) cells in the oculomotor vermis (OMV, lobules VIc and VII) are thought to play important roles in real-time saccade control (Herzfeld et al., 2015). These neurons project to the caudal fastigial nucleus (cFN) which, in turn, project to premotor burst neurons in the saccade burst generator (SBG) (Noda et al., 1990). OMV P-cells are therefore positioned to optimize saccade speed and accuracy given the demands of oculomotor mechanics. How this modification is accomplished is not yet understood.

[Figure 1]

According to a popular local feedback model (Fig. 1), a desired saccade displacement command drives excitatory burst neurons (EBN), which, in turn, activate motoneurons (MN) to move the eyes quickly to the intended target (Robinson, 1975; Jürgens et al., 1981). This feedforward pathway produces the force needed to obtain a peak velocity that is optimal for the intended saccade displacement (Robinson, 1964; Harris and Wolpert, 2006). To account for the viscoelastic properties of the eyes, the feedforward pathway contains an inverse model of the oculomotor plant to produce a burst that compensates for these mechanics. The inverse model is thought to reside in the cerebellum (Wolpert et al., 1998).

A second component of the model is a feedback pathway that integrates an efference copy of the EBN command to predict the displacement of the eyes. When the difference between the predicted and desired displacement (the dynamic motor error or DME, Fig. 1) reaches zero, the saccade stops. This model explains how saccade accuracy is maintained despite midflight perturbations (Keller et al., 1996; Xu-Wilson et al., 2011) or pharmacological slowing (Soetedjo et al., 2002; Barton et al., 2003). This feedback circuitry also may involve the cerebellum (Quaia et al., 1999).

A key difference between the feedforward and feedback pathways is that manipulations of the former are compensated by the latter to keep movements accurate. A second difference between them is that the feedback pathway has less direct access to the EBNs and may involve more synapses. We exploited these differences to ask whether OMV P-cells/cFN neurons contribute to the feedforward pathway, the feedback pathway, or both. Specifically, we expressed channelrhodopsin (ChR2) in the OMV P-cells of two macaques (El-Shamayleh et al., 2017) and activated these neurons with brief light pulses at different times during visually guided saccades.

These perturbations deviated saccade trajectories in ways that depended on saccade direction. Contraversive saccades were slowed in midflight after a short latency, and this deceleration was followed by a compensatory reacceleration that brought the eyes to the target. Both effects are consistent with a reduced drive in the feedforward pathway. In contrast, stimulation during ipsiversive saccades prolonged their deceleration phase, largely independently of when the stimulation was applied. Stimulation-perturbed saccades were systematically hypermetric, and the amount of hypermetria scaled with light pulse duration. These effects are consistent with a reduced drive at the input of the feedback integrator. We conclude that the role of the OMV in saccade control depends on the direction of the saccade: the contralateral OMV is part of the feedforward pathway whereas the ipsilateral OMV is part of the feedback integrator. Our conclusion is supported by a detailed version of the saccade generator model (Fig. 1) under which stimulation of feedback and feedforward pathway produces perturbed eye movement trajectories that closely match those produced by actual brief activation of the ipsi- and contraversive OMV, respectively.

Materials and Methods

All experiments were performed in accordance with the Guide for the Care and Use of Laboratory Animals and exceeded the minimum requirements recommended by the Institute of Laboratory Animal Resources and the Association for Assessment and Accreditation of Laboratory Animal Care International. All the procedures were evaluated and approved by the local Animal Care and Use Committee of the University of Washington.

Animal subjects. Two juvenile male rhesus monkeys (*Macaca mulatta*), Sq and Tm (8.1 and 12.9 kg, respectively), participated in this study. Animal Sq, but not Tm, had participated in previous studies (El-Shamayleh et al., 2017; Soetedjo et al., 2019). Both animals underwent two surgeries; the first was to implant a scleral search eye coil (Judge et al., 1980) and head stabilization lugs. The second was to implant stainless steel recording chambers, one aimed at the superior colliculus (SC) and the other at the OMV. The OMV chamber was aimed straight down, 3 mm left of the midline and 14 mm posterior in Sq and 1.5 mm left of the midline and 15 mm posterior in Tm, relative to the stereotaxic ear-bar zero.

After the animals had recovered from the first surgery, they were trained to track a red laser dot (~0.25° diameter) on a tangent screen 62 cm from their eyes. To obtain a dollop of fortified applesauce reward, the animals were required to fixate the dot for 1.2 – 2 sec, and after the target spot jumped, to shift their gaze to the target in <450 ms and remain within (± 2°) of the target for 1.5 sec. Once they performed this task reliably for ≥2 hours, the recording chambers were implanted.

AAV vector Injection. Adeno-associated virus (AAV) shuttle plasmid engineering and vector production has been described previously (El-Shamayleh et al., 2017). AAV vectors were injected as follows. Using standard extracellular recording techniques, we identified the OMV on the basis of saccade-related activity and then mapped the spatial extent accessible within

the recording chamber (Soetedjo and Fuchs, 2006; Soetedjo et al., 2008; Kojima et al., 2010). We injected the AAV vector solution using an injectrode made of 30 G stainless steel hypodermic tubing insulated with polyimide and epoxylite (Kojima et al., 2021; Soetedjo and Kojima, 2022). We injected the AAV vector solution at depths with strong saccade-related multiunit activity. Sq received a total of 24 µL of AAV9-L7-ChR2-mCherry (1.41×10^{13} genomes/mL) across 4 tracks (~0.75 mm apart) and at up to 4 depths per track (1.5–2 µL at each depth over the course of 1 min with ≥ 2 min between injections) (El-Shamayleh et al., 2017). Tm received a total of 27 µL of AAV1-L7-ChR2-mCherry (1.53×10^{13} genomes/mL) along a single track at 7 depths (3–5 µL at each depth over the course of 2 min with ≥ 3 min between injections). We waited at least 6 weeks after the injection to start experiments.

Saccade task. Sq and Tm were trained to make horizontal 24° saccades that started from a 12° eccentricity and crossed straight-ahead gaze. To reduce target predictability, approximately 30% of the steps were either 6 or 18°. These “catch” trials were not accompanied by light activation and were not analyzed. When a saccade onset was detected, the target spot was extinguished for 200 ms to eliminate the possibility of any visually guided corrective movement following primary saccades.

[Figure 2]

Light activation. We stimulated ChR2-expressing P-cells with a custom built 450 nm light source based on an Osram PLTB450B laser diode (El-Shamayleh et al., 2017; Soetedjo and Kojima, 2022) coupled to a 200 µm, 0.39 NA (FT200EMT, Thorlabs, Newton, NJ, USA) optical fiber patch cable. To minimize tissue damage and increase light spread, the optical fiber was sharpened to an apical angle of 20°. A double-barrel cannula housed an Alpha-Omega glass-tungsten microelectrode (impedance: ~100 kΩ at 1 kHz) and the optical fiber. The microelectrode was used to identify depths with strong saccade-related activity. The electrode

and optical fiber were driven independently using an EPS micro-positioner (Alpha-Omega, Nazareth, Israel). During experiments, the tip of the fiber was 0.5–1 mm above the tip of the microelectrode.

We performed two types of experiment that differed in light pulse duration. In the first type, which was performed on both animals, the light pulse was triggered at one of 4 different times relative to saccade onset detection. The first was as early as possible (0 ms delay); we call this light pulse "T0". The second, third and fourth trigger times occurred 10, 20, and 30 ms after T0 (T10, T20 and T30, respectively). T0 and T10 occurred during the saccade acceleration phase, T20 occurred near the time of peak velocity and T30 occurred during the deceleration phase. In these experiments, light pulse duration was fixed at 30 ms for Sq and at 10 ms for Tm. The briefer pulses in Tm were motivated by the need for more precise estimates of effect latency, which differed for ipsilateral and contralateral saccades. To provide approximately equal light flux to each animal, the optical power of the laser was set to 60 mW for Sq and to 130 mW for Tm. In the second experiment type, performed on Tm only, light pulse durations varied randomly across four values: 1.25, 2.5, 5 and 10 ms. In these experiments, light pulses were delivered at T0 only.

The light source was triggered by saccade initiation (Fig. 2). Saccades initiation was detected by a Power 1401 data acquisition and control system (Cambridge Electronic Design, UK) that monitored horizontal eye velocity continuously. When the eye velocity after a target step crossed a 15°/s threshold, the Power 1401 randomly picked a trigger time and produced a TTL pulse. In the first experiment type, 4 trigger times were used (T0–T30), and the TTL pulse drove the laser directly. In the second type, the Power 1401 generated a TTL pulse at time T0 that triggered an Arduino microcontroller which randomly produced a 1.25, 2.5, 5 or 10 ms pulse that drove the laser. The delay introduced by the Arduino was ~100 µs.

General data analysis. All data were saved in Spike2 (Cambridge Electronic Design, UK) format, and analyses were performed in Spike2 and Matlab (Mathworks, USA). Eye and target position data were digitized at 1 kHz. Extracellular voltages and signals from a laser-detecting photodiode were digitized at 50 kHz. The on and off times of each laser pulse were extracted from the sampled photodiode output. Eye position traces were filtered forward and backward (Matlab “filtfilt” function, non-causal) with a 70 Hz, low pass, 61-coefficient Hamming window finite impulse response filter to reduce recording noise. A central derivative (Matlab “gradient” function) was applied successively to the filtered eye position signal to obtain eye velocity and then acceleration. After each target step, the program searched the subsequent 90–500 ms for an eye velocity >50 °/s and identified the first such movement, if it existed, as a saccade. Horizontal eye velocities that rose above, or fell below, a threshold of 15 °/s were considered the onset and termination of the saccade, respectively. The program identified the amplitude of the target step and measured the metrics of the saccades, as well as the occurrence times of light pulses. We discarded trials that were contaminated by blinks and those in which the horizontal or vertical eye position was ≥1.5° from the target when it stepped. These two criteria eliminated <10% of the trials.

Determining optogenetic effect latency. To measure the latency of optogenetic stimulation on saccades, we divided trials into five groups: control (no light pulse), T0, T10, T20 and T30. We aligned the position, velocity and acceleration traces on saccade onset (the time at which eye velocity exceeded 15 °/s) and averaged them within each group for each saccade direction. The light pulse onset time was defined as the mean time of occurrence of the light pulse within each condition. The standard deviations of the onsets ranged from 0.54 to 1.22 ms (Tables 1 and 2).

We compared eye acceleration on control trials against those in each stimulation group using a 2-tailed Student's t-test (Matlab “ttest2” function with default options) each millisecond

from the light pulse onset time until 125 ms after saccade onset. We considered the light pulse to have had an effect on conditions in which the P values were <0.05 for at least 10 consecutive milliseconds. The first time at which P=0.05 was estimated using a 2-point linear interpolation. To estimate the mean occurrence time of the effect, we performed a bootstrap analysis on the light-perturbed trials in each group. We obtained 1000 resampled (with replacement) data sets and compared each of these bootstrap data sets with the control data set to obtain an estimate of the time of the effect as described above.

Normalization for population analysis. To pool data across experiments, we calculated a pair of normalization factors for each experimental session, one for rightward saccades and one for leftward saccades, that compensated for small changes in the gain of the eye coil system across days. In each trial, we set the horizontal eye position, measured 10 ms before the identified onset of the saccade, to zero. We presumed that the eyes were nearly stationary or nearly so during this epoch. We then computed the mean saccade amplitude from control trials in each experiment using the eye position 125 ms after saccade onset as the endpoint. We then normalized this mean saccade amplitude of the control trials to exactly 24°. We then multiplied each position, velocity and acceleration trace by the normalization factor.

Statistics. Hypothesis testing for the comparison of saccade metrics, e.g., amplitudes, peak velocity and duration, was performed using a permutation test with 10,000 iterations (Wilcox, 2022). We considered P<0.05 as significant for all statistical tests. Averages (mean ± SD) were computed across trials within each condition. The standard deviation of the difference between the means was computed as: $SD = \sqrt{(SD_c^2 + SD_s^2)}$ (Taylor, 1997), where SD_c is the standard deviation in the control conditions and SD_s is the standard deviation in the stimulation condition. Bonferroni correction was used to control the Type I error rate of multiple comparisons between control trials and the four stimulation conditions (T0, T10, T20 and T30). Other statistical tests are described in the Results as needed.

Quantitative model description. We compared the effects of OMV P-cell activation with simulations from a local negative feedback model of saccade burst generator (Fig. 13A). The model was constructed in Simulink, a Matlab graphical block diagramming tool for simulating dynamical systems. Model simulations used a 4th order Runge-Kutta ordinary differential equation solver with 0.1 ms time step. Starting from the eyes, the eye plant block transfer function was (Robinson, 1964; Fuchs and Luschei, 1971; Goldstein and Robinson, 1984; Fuchs et al., 1988; Scudder, 1988):

$$E(s) = \frac{0.075s+1}{(0.25873s+1)(0.029852s+1)(0.0034181s+1)} \quad (1)$$

The motoneurons were implemented as a summing block that receives excitatory inputs from position integrator (step), EBNs (pulse) and a slide component transfer function (slide) with the following weights: *wIntMN* = 0.988, *wEbnMN* = 0.104 and *wSlideMN* = 0.1092, respectively (see Fig. 13A for weight locations in the model). The slide component transfer function was:

$$S(s) = \frac{1}{0.075s+1} \quad (2)$$

At the input of the EBN and OPN blocks, we placed a first-order low pass filter with a 2 ms time constant to simulate synaptic-input temporal integration:

$$G(s) = \frac{1}{0.002s+1} \quad (3)$$

The EBN firing rate (*EBNfr*) was computed as:

$$EBNfr(x) = \begin{cases} MaxEBNfr(1 - e^{-0.0009x}) & for\ x \geq 0 \\ 0 & for\ x < 0 \end{cases} \quad (4)$$

Maximum EBN firing rate (*MaxEBNfr*) was set to 1000 spikes/s to simulate fast saccades, and 750 spikes/s to simulate slow saccades. The OPN firing rate (*OPNfr*) was computed as:

$$OPNfr(x) = \begin{cases} 160 & for\ x > opn\ threshold \\ 0 & for\ x \leq opn\ threshold \end{cases} \quad (5)$$

The value of *opn threshold* was set to 50 spikes/s. The OPNs inhibited the EBNs with a weight of *wOpnEbn* = 32.

The IBNs were implemented as a summing block that receives excitatory inputs from EBNs and OPN trigger (150 spikes/s 10 ms pulse). The IBNs inhibited the OPNs with a weight of *wIbnOpn* = 1.50. To convert the dynamic motor error (DME) output from the comparator to a firing rate, a weight of *wCompEbn* = 80 was used. A 5-ms delay (transfer function $e^{-0.005s}$) followed the feedback integrator ($\frac{1}{s}$) (Van Gisbergen et al., 1981). All weight values were chosen to produce 24° saccades with velocity profiles that approximated data in Fig. 10.

To simulate a 24° saccade, a step was applied to the comparator, and an OPN trigger occurred 40 ms later. To simulate T0 or T20 optogenetic light activation of OMV P-cells, a 450 spikes/s, 10-ms pulse occurred at either 6.4 ms or 26.4 ms after saccade onset, respectively. The pulse was applied at the negative input of either the EBNs to represent contraversive perturbation, the feedback integrator to represent ipsiversive perturbation, or both to represent midline perturbation of OMV P-cells.

Code accessibility

Model and its associated codes are available through Github:

https://github.com/robisoe/OMV_L7_paper_model

Results

We performed 18 experiments with light pulses at four delays with respect to saccade onset (8 experiments in Sq, 10 in Tm). Significant effects on saccade metrics were obtained in all of these experiments except one (Fig. 4C, “+”) which was not analyzed further.

Effects of T0 light pulses on saccade metrics and kinematics. Optical stimulation of OMV P-cells produced distinct effects on leftward and rightward saccades. In an exemplar experiment from Sq (Fig. 3A, B; leftward triangle in Fig. 4C, left panel), T0 light pulses triggered by *leftward* saccades (5.34±0.92 ms) (Fig. 3A, blue bar) did not affect the peak saccade velocity (P=0.77), but caused a reacceleration ~36 ms after pulse onset, during the deceleration phase (Fig. 3A bottom panel, vertical line). This reacceleration extended saccade duration by 7.18±8.41 ms, and increased saccade amplitude by 2.19±1.13°.

In contrast, T0 laser pulses triggered by *rightward* saccades (5.18±0.91 ms after saccade onset, Fig. 3B) reduced eye velocity ~11 ms after pulse onset. This latency was roughly one third of the latency on leftward saccades. This slowing of the saccade reduced peak eye velocity by 120.73±127.96 °/s (P<0.0001), but the amplitude loss during acceleration (4.49±2.36°) was compensated for by an amplitude increase during deceleration (3.92±3.56°). Consequently, saccades were normometric (amplitude change relative to control: -0.57±2.68°, P=0.32).

[Figure 3]

Similar effects were obtained from animal Tm (Fig. 3C, D; square in Fig. 4C, right panel). T0 light pulses triggered by *leftward* saccades (Fig. 3C) reduced eye velocity ~7 ms after pulse onset, decreasing peak velocity by 88.46±113.83 °/s (P<0.0001). The reduction of peak velocity was followed by a reacceleration that increased the displacement during deceleration by 3.34±2.28°, which compensated the amplitude loss of 3.63±2.19° during the acceleration phase

and resulted in normometric saccades (P=0.24). These data, obtained from Tm during *leftward* saccades, are similar to those obtained from Sq during *rightward* saccades (Fig. 3B).

The effects of T0 light pulses on Tm's *rightward* saccades (Fig. 3D) were similar to those on Sq's *leftward* saccades (Fig. 3A). The light pulses did not affect the peak velocity (P=0.92), and reacceleration started ~23 ms after pulse onset, increasing saccade amplitude by 1.57±0.97° (P<0.0001).

[Figure 4]

The dependence of these effects on saccade direction is reminiscent of the hyper- and hypometric saccades produced by inactivation of the ipsi- and contralateral CFN, respectively (Robinson et al., 1993; Iwamoto and Yoshida, 2002; Goffart et al., 2004). OMV P-cells project to the CFN in an uncrossed manner (Noda et al., 1990), suggesting that our results might depend on the media-lateral location of the optical fiber in the OMV (Fig. 4A). As the optical fiber was moved from more central (0) to lateral locations in the vermis of Sq, the amplitude of leftward saccades increased (Fig. 4A, left, black circles) and the amplitude of rightward saccades decreased (red circles). T0 pulses delivered near the midline (two filled circles) produced small hypermetrias for both left- and rightward saccades (all P<0.06) that did not differ significantly (P>0.4). In Tm, as stimulation locations moved from lateral to central vermis positions, the amplitude of rightward saccades decreased (Fig. 4A, right, red circles) whereas the amplitude of leftward saccades increased (black circles). At the two locations to the left of the midline (filled circles), optogenetic stimulation did not produce a significant difference in amplitude change for either rightward or leftward saccades (P>0.1).

These analyses suggest that the OMV recording chambers were slightly off-center. In Sq, the chamber was slightly to the left of the functional midline, and in Tm, the chamber was slightly to the right. We therefore describe Sq's leftward saccades, and Tm's rightward

saccades, as *ipsiversive*. We describe Sq's rightward saccades, and Tm's leftward saccades, as *contraversive*. Chamber locations for all experiments are shown in Fig. 4C (gray circles). For the purposes of population analyses, we pooled experiments conducted at the leftmost chamber locations (Fig. 4B, left, open circles) in Sq with those conduced at the rightmost chamber locations in Tm (Fig. 4B, right, open circles).

Effects of laser pulse time on ipsiversive saccades. Laser stimulation affected the deceleration phase of ipsiversive saccades, largely irrespective of pulse timing. Despite the 10 ms delay between them, T0 and T10 pulses produced reaccelerations that occurred at approximately the same time. With respect to saccade onset, these effects occurred at 35.62±0.97 and 36.16±1.18 ms for Sq and at 27.89±0.89 and 29.70±1.18 ms for Tm (Fig. 5A, C, red and green vertical lines). With respect to laser pulse onset, these times correspond to latencies of 30.76±0.97 and 21.27±1.17 ms for Sq and to 20.66±0.89 and 12.53±1.18 ms for Tm (Table 1). In summary, T0 and T10 pulses produced a reacceleration that was more closely time-locked to the movements than it was to the timing of the light pulses.

[Figure 5]

[Table 1]

In contrast to T0 and T10 pulses, which affected saccades at approximately the same time, T20 and T30 pulses affected saccades later (Fig. 5B, D, blue and brown vertical lines). After T20 pulses, reacceleration occurred 38.64±0.73 (34.06±3.29) ms after saccade onset, for Sq (Tm), which is ~2.5 (4.5) ms later than it did following T10 pulses. Reacceleration after T30 pulses occurred 45.28±1.18 (43.59±2.39) ms after saccade onset for Sq (Tm), which is ~7 (10) ms later than it did after T20 pulses. Therefore, the onset of reacceleration was more dependent on the light pulse timing when pulses are delivered later during the saccade.

Change in saccade metrics. Optical stimulation caused ipsiversive saccades to become hypermetric (Fig. 5A-D, top panels; Table 1), but did not affect peak velocity (one-way ANOVA across control and T0–T30 groups: $F<1.5$, $P>0.1$, both animals), acceleration duration ($F<1.7$, $P>0.1$, both animals), or displacement amplitude of the eye during the acceleration phase ($F<1.3$, $P>0.1$, both animals). It did, however, increase deceleration duration ($P<0.0001$, all conditions except for T0 and T10 in Tm for which $P>0.15$). Therefore, eye displacement during the deceleration phase increased (all P values <0.0001; Table 1).

[Figure 6]

Titrating the reacceleration effects. To determine whether saccade amplitudes were also dependent on pulse duration, we fixed the start time of the laser pulse at T0 and varied its duration from 1.25 to 10 ms (Tm only). Despite their brevity, 1.25 ms pulses extended ipsiversive saccades by 0.75±0.92° ($P<0.0001$), demonstrating the remarkable effectiveness of this optogenetic manipulation on primate behavior (Fig. 6A, B). Increasing the light pulse duration produced yet larger saccades (Fig. 6B, red line, slope: 0.22 °/$\log_2$[pulse duration], $P<0.0001$).

In summary, brief activation of ipsilateral OMV P-cells reaccelerated saccades during their deceleration phase and produced hypermetria. The time at which reacceleration occurred depended on the state of the movement but relatively little on stimulation timing. Hypermetria increased with the duration of the stimulation, which is consistent with an integration mechanism. These results contrast with the effects of OMV P-cell activation on contralateral saccades, which we describe below.

Effects of laser pulse time on contraversive saccades. As shown in Fig. 3B and C, the main effect of the light pulse on contraversive saccades was a deceleration which was followed by reacceleration that compensated for it. The onset of this deceleration was strongly dependent on light pulse timing. For Sq, T0, T10, and T20 pulses decelerated saccades starting at 13.86±0.71, 22.76±0.69 and 31.63±1.85 ms after saccade onset, respectively (Fig. 7A, B, vertical lines; T30 pulses (brown bars) had no significant effect). Relative to laser onset, the latencies were ~6–9 ms (Table 2). Similar results were obtained for Tm; in this animal, T0, T10, T20, and T30 pulses decelerated saccades with a latency of ~4–5 ms (Table 2; Fig. 7C, D, vertical lines). These results show that OMV stimulation decelerates contraversive saccades at low latency irrespective of the state of the movement.

[Figure 7]

[Table 2]

Change in Saccade Metrics. T0 pulses reduced the peak velocity of contraversive saccades by 106.61±130.27 °/s in Sq and by 97.43±114.27 °/s in Tm, (both P<0.0001; Fig. 7A, C, velocity panels, red traces; Table 2). Under most circumstances, lower velocities are associated with shorter saccades. The standard relationship between peak velocity and amplitude (the main sequence, (Bahill et al., 1975)) predicts a 5° smaller amplitude in response to a 10% decrease in the peak velocity of a 24° saccade (Fuchs, 1967). Despite the nearly 15% reduction of peak velocity produced by optogenetic OMV P-cell stimulation, the amplitudes of contraversive saccades remained relatively unchanged. We note that saccade amplitude decreased slightly but significantly in Sq (by 0.93±2.18°, P<0.001, Fig. 7A, position panel, red trace), but this decrease is small relative to that expected from the main sequence. No significant change was found in Tm (P=0.39, Fig. 7C, position panel, red trace; Table 2).

T0 optogenetic stimulation abbreviated the acceleration phase of contraversive saccades, decreasing eye displacement during this phase by 3.07±2.51 and 3.77±2.17° in Sq and Tm, respectively (Table 2). To compensate for this amplitude loss, the eyes reaccelerated at 35.83±0.95 and 26.18±0.39 ms after saccade onset for Sq and Tm, respectively (Fig. 7A and C, acceleration panels, red traces). Increasing the duration of the T0 pulse from 1.25 to 10 ms slightly reduced acceleration displacement (three experiments in Tm). Nevertheless, saccade reacceleration during the deceleration phase compensated for the displacement loss so that saccade amplitude was nearly constant for all pulse durations (one-way ANOVA across control and all 4 pulse duration groups: $F(4, 803)=2.08$, $P=0.081$). These data attest to the engagement of a mechanism that extends the deceleration phase to compensate for an abbreviated acceleration phase.

[Figure 8]

The negative feedback model (Fig. 1) predicts that, for a given saccade amplitude, saccade duration should decrease as peak velocity increases (Soetedjo et al., 2002; Barton et al., 2003). Linear regression confirmed this prediction and showed that the peak velocity of contraversive control saccades explained >60% of the variation in saccade duration (Fig. 8A, B, black circles and lines, R^2=0.61 and 0.73 for Sq and Tm, respectively). When light pulses were applied at T0 and T10, the relationship between saccade duration and peak velocity still was nearly linear (T0: Fig. 8A, B, red lines, R^2=0.70 and 0.62, for Sq and Tm, respectively) and (T10: Fig. 8C, D, green lines, R^2=0.69 and 0.58, for Sq and Tm, respectively) although the relationship became steeper. In summary, the slowing of contraversive saccades was accompanied by increased duration as predicted by the negative feedback model.

[Figure 9]

A similar analysis of saccades following T20 and T30 light pulses, which occurred during saccade deceleration, revealed a distinct relationship between the peak velocity and deceleration duration of stimulated saccades in comparison to control saccades. For a given saccade amplitude, slower saccades had longer deceleration durations. (Fig. 9A-C, control saccades, black circles and linear regression lines: R^2= 0.30 and 0.53 for Sq and Tm, respectively). On stimulated trials, slow saccades had unusually long deceleration durations, and the relationship between peak velocity and deceleration duration on stimulated trials was fit better with a second-order polynomial than by a line (Fig. 9A-C, blue and brown data and fits, F-test, P<0.0001). Saccade deceleration duration decreased steeply with increasing peak velocity, and deceleration durations on some stimulation trials were shorter than those of controls. These results suggest that late OMV P-cell activation truncated the fastest contraversive saccades, but prolonged the deceleration phase of the slower ones. An analysis of saccade velocity profiles confirmed these results; T20 and T30 pulses decelerated contraversive saccades, and truncated the fast ones selectively (Fig. 10).

[Figure 10]

The selective truncation of fast saccades may be related to the fact that the gaze was relatively close to the intended target when the pulse occurred. Consistent with this idea and as expected, the average eye displacement when the pulse occurred during fast saccades (10.36±1.51°, 12.26±0.80° and 18.04±0.87° for trials in Fig. 10A-C, respectively) was larger than during slow saccades (7.30±1.47°, 7.58±0.93° and 11.01±1.80° for trials in Fig. 10D-F, respectively; all P values <0.0001). Truncated fast saccades were hypometric (Fig. 10A-C, insets, all P values <0.01), but slow saccades were near normometric (Fig. 10D-F, insets, all P values > 0.2).

Mixed contra- and ipsiversive effects after midline stimulation. In four experiments (two on Sq and two on Tm), we delivered light pulses near the midline vermis (Fig. 4A, B, filled circles). These produced mixed effects. As before, we compared the population average time courses of eye position, velocity and acceleration (Fig. 11, Sq: A, B, E, and F; Tm: C, D, G and H). For consistency, the ipsiversive direction was defined as leftward for Sq and rightward for Tm, and we present the data in the same directional order as in Figs. 5 and 7 (Fig. 11A – D, ipsiversive; E – H, contraversive).

[Figure 11]

In both animals, T0 light pulses reduced the peak velocity of both ipsi- and contraversive saccades (Fig. 11A, C, E and G, middle panels, red traces, $P<0.0001$). The reduction in peak velocity, consistent with the contraversive effect, was followed by reacceleration that produced small, but significant, hypermetria, consistent with the ipsiversive effect (1.23±1.54, 0.41±1.47, 1.08±1.99 and 0.38±1.35°; Fig. 11A, C, E and G, respectively, $P<0.031$). T10 pulses also significantly decelerated both left- and rightward saccades (green traces) at short latency and caused a reacceleration at longer latency. Saccades in this condition tended to be hypermetric (all except Sq's rightward saccades, Fig. 11A, C and G; $P<0.0001$). Similar results were obtained on T20 and T30 stimulation trials (Fig. 11B, D, F and H). No hypometria was produced in either direction for any pulse condition in either animal.

Does the ipsilateral OMV help compensate for the effects of contralateral activation? T0-perturbed contraversive saccades exhibited a compensatory reacceleration during their deceleration phase that brought the saccades closer to normometric (Fig. 7; Table 2). An intriguing possibility is that the ipsilateral OMV/cFN was responsible for the compensatory reacceleration of perturbed contraversive saccades.

To test this possibility, we compared the time of occurrence of the ipsiversive effects (Fig. 12A, B, respectively) with the time of the compensatory reacceleration of perturbed contraversive saccades (Fig. 12C, D, respectively). We analyzed T0 data because they exhibited the earliest and largest effect on peak velocity.

[Figure 12]

We examined the times at which the compensatory reacceleration occurred (Fig. 12C, D, green lines; same as red arrows in Fig. 7A, C). For Sq, this occurred 35.83±1.90 ms after the onset of perturbed contraversive saccades (mean±2SE, Fig. 12C, green solid and dashed lines). In comparison, the effect of T0 pulses on ipsiversive saccade occurred 35.62±1.95 ms after saccade onset (Fig. 12A, blue solid and dashed lines). These two times differ by <1 ms. The same comparison for Tm yielded similar results, compensatory reacceleration occurred 26.18±0.78 ms after the onset of a contraversive saccade (Fig. 12D, green solid and dashed lines) and T0 pulses affected ipsiversive saccades 27.89±1.77 ms after saccade onset (Fig. 12B, blue solid and dashed lines). These results are consistent with the idea that the ipsilateral OMV/cFN is part of the circuit that compensates for the decrease in the contraversive velocity caused by contralateral OMV P-cell activity.

Comparison with model simulations. The short latency of contraversive effects is consistent with OMV P-cells being in the feedforward path of the local feedback model of the saccade generator. This placement is also supported by the compensation that occurred after optogenetic perturbations; this compensation is similar to that observed after electrical stimulation of omnipause neurons (OPN) (Becker, 1981; Keller et al., 1996) and the inactivation of pontine saccadic premotor neurons (Soetedjo et al., 2002; Barton et al., 2003), which are in the feedforward path. In contrast, optogenetic perturbation of ipsiversive saccades occurred at

a long latency, appeared to accumulate with longer pulse durations, were uncompensated, and led to hypermetria. These data suggest that the ipsilateral OMV may contribute to the feedback path.

[Figure 13]

We formalized these intuitions using a local feedback model of the saccade generator that included a “latch” circuit to prevent the OPN from firing during a saccade (Fig. 13A, see Methods for detail quantitative description of the model) (Fuchs et al., 1985; Takahashi et al., 2022). The input of the model is a 24° displacement command, which is compared with the estimate of eye displacement from the feedback integrator to produce a dynamic motor error (DME). During fixation, the OPNs inhibit both EBNs and inhibitory burst neurons (IBNs) (Langer and Kaneko, 1983; Iwamoto et al., 2009). A trigger signal (10 ms black pulse, 150 spikes/s), presumably from the superior colliculus (Sparks et al., 2000), inhibits the OPNs via the IBNs (Takahashi et al., 2022) and allows the EBNs to respond to the DME. The EBNs drive the abducens motoneurons (MNs) directly to produce the burst that accelerates saccades. In addition, the EBNs drive the MNs via a position integrator (Kaneko, 1997) to produce a steady firing rate (a step) to hold the gaze where the saccade lands and also via a transfer function to produce the decaying part (“slide” term) of abducens firing rate before reaching a steady rate to prevent post-saccadic drift (Collins et al., 1975; Optican and Miles, 1985; Sylvestre and Cullen, 1999). The EBNs also drive both the feedback integrator and the IBNs (Sasaki and Shimazu, 1981; Strassman et al., 1986a) which in turn, inhibits the OPNs. The EBN-IBN-OPN-EBN loop forms a latching circuit that maintains the OPN’s pause during a saccade.

The cFN, which projects to both the contralateral EBNs and IBNs, is inhibited by OMV P-cells. Therefore, optical activation of the contralateral vermis was implemented in the model as a 10 ms 450 spikes/s pulse that inhibited the EBNs. How the ipsilateral cFN influences the

burst generator is less clear because because the targets to which it projects, the contralateral EBNs and IBNs, are silent during ipsiversive saccades due to inhibition by ipsilateral IBNs (Strassman et al., 1986b; Takahashi et al., 2022). Because our data showed that the effect of ipsilateral OMV P-cell stimulation appeared to be integrated and produced hypermetria, we applied a 10 ms 450 spikes/s pulse (brown) with a negative weight to inhibit the feedback integrator.

Contralateral OMV P-cell activation that occurs 6.4 ms after saccade onset (Fig. 13B, red bar) decelerates saccades at a short latency (Fig. 13B, velocity panel, compare black control and red perturbed saccades). Shortly after the end of this pulse, the saccade reaccelerates and lands on target due to the feedback circuit (Fig. 13B, position and velocity panels, red trace). The same activation pulse creates similar effects on slow saccades (Fig. 13C, red traces).

The effects of activation pulses that occur during the deceleration phase (26.4 ms after saccade onset, Fig. 13B, C, blue bar) depend on the speed of the saccades. The pulse decelerates both fast and slow saccades, but fast saccades do not reaccelerate and become hypometric (Fig. 13B, blue trace). In contrast, slow saccades reaccelerate and fully compensate for the deceleration (Fig. 13C, blue trace). During a slow saccade, the DME decreases more slowly than it does during a fast saccade (DMEs at blue pulse onset are 8.55 and 12.13° for fast [Fig. 13B] and slow saccades [Fig. 13C], respectively). The slower decrease of the DME slows the decrease of EBN activity, which prevents the OPN input from exceeding the 50 spikes/s threshold to resume firing during the activation pulse. The saccade reaccelerates and is normometric. These model simulations recapitulate the results shown in Fig. 10.

Ipsilateral activation reduces the “charge” in the feedback integrator and produces reacceleration during the deceleration phase of the saccade (Fig. 13D, red and blue traces). The latency of the reacceleration is attributed to a 5 ms delay in the feedback path; therefore, the model produces the same latencies for early (red bars) and late (blue bar) activation pulses. This is an imperfect reflection of reality: the latency of ipsilateral OMV P-cell activation decreased when activation occurred later (Table 1). This decreasing latency suggests a delay mechanism that depends on the real-time state of the saccades.

Delivering *both ipsi- and contralateral* activating pulses to the model *simultaneously* produces saccades that mimic the mixed effect produced by activation of the midline vermis (compare Figs. 11 and 13E). An early contralateral activation pulse (red bar) reduces peak velocity, but the simultaneous ipsilateral activation pulse causes the model to over-compensate and produces hypermetria (Fig. 13E, red traces). A later contralateral activation pulse truncates fast saccades (Fig 13B, blue), but simultaneous ipsilateral activation prevents this truncation (Fig. 13E, blue bar). The simultaneous ipsilateral activating pulse decreases the output of the feedback integrator, thereby increasing DME. This DME increase balances the simultaneous contralateral activating pulse, which in turn, prevents the OPN from being activated. The reacceleration after the pulse over-compensates, leading to hypermetria (Fig. 13E, blue traces). We also did not observe saccade truncation in the experimental midline stimulation, and the perturbed saccades were either hypermetric or normometric (Fig. 11).

In conclusion, the qualitatively similar responses produced by activation pulses on an established local feedback model suggest different roles for the contra- and ipsilateral OMV/cFN complex in saccade generation. The contralateral side contributes to the feedforward path, influencing the saccade at short latency, whereas the ipsilateral side contributes to the feedback path, integrating EBN activity and balancing the contralateral drive to allow the saccade to land on target.

Discussion

Our results show that brief activation of OMV P-cells during a saccade changes its trajectory in midflight. The nature of the change depends on the direction of the saccade relative to the locus of stimulation. Stimulation during contraversive saccades produced a deceleration within ~6 ms. If stimulation occurred near saccade onset, a compensatory reacceleration occurred during the deceleration phase, driving the saccades to land on or near the target. If stimulation occurred later, the compensatory reacceleration was velocity-dependent. Slower saccades reaccelerated and landed near the target. Faster saccades did not reaccelerate and were hypometric.

In contrast, OMV P-cell stimulation affects ipsiversive saccades at a longer delay. Under these circumstances, reacceleration during the saccade deceleration phase was not followed by compensation, so saccades were hypermetric. The amount of hypermetria grew with the duration of the activation pulse.

Circuitry underlying the effects on contraversive saccades

What is the effect of OMV P-cell activity on the SBG? OMV P-cells inhibit neurons in the cFN, which project to contralateral pontine and medullary burst neurons. During saccades, the cFN drives contralateral EBNs and IBNs in the SBG. The EBNs, in turn, drive ipsilateral abducens motoneurons, and IBNs inhibit contralateral abducens motoneurons.

This circuit predicts the results of contralateral OMV P-cell activation. The light pulse excited P-cells, inhibiting the cFN and reducing its drive to both EBNs and IBNs. Reduced activity in the EBNs and IBNs reduced the drive to the agonist abducens motoneurons and the inhibition of the antagonist abducens motoneurons, respectively. A short-latency slowing of the

saccade is therefore expected. Given that the shortest latency of a simple spike following a light pulse is ~3 ms (El-Shamayleh et al., 2017), we conclude that the excited P-cells decelerates contraversive saccades within ~3 ms.

Two additional observations support the idea that the contralateral P-cell activation reduced the activity of the feedforward element of a local feedback model (Robinson, 1975; Jürgens et al., 1981). First, T0 activation pulses slowed saccades but did not lead to hypometria. A reacceleration during the deceleration phase compensated for the displacement reduction during the acceleration phase. This effect is similar to those produced by brief OPN stimulation (Becker, 1981; Keller et al., 1996), and OPNs are known to inhibit neurons in the feedforward pathway (Langer and Kaneko, 1983; Strassman et al., 1987; Iwamoto et al., 2009).

Second, late activation pulses (T20 and T30), which occur during the saccade deceleration phase, truncate faster saccades. The local negative feedback model readily explains this phenomenon. The faster the saccade is, the lower the DME is when the activation occurs. Low DME breaks the OPN latch circuit (Van Gisbergen et al., 1981; Scudder, 1988; Yoshida et al., 1999; Takahashi et al., 2022), allowing the OPNs to become active, thereby stopping the saccade. Our results suggest that contralateral OMV P-cell activity during saccade deceleration phase can control saccade termination, likely via OPN reactivation. In summary, our data make a strong case that contralateral OMV P-cells control the activity of feedforward neuronal elements of the pontine burst generator.

Circuitry underlying the effects on ipsiversive saccades

In contrast to contralateral activation, ipsilateral activation produced hypermetric (non-compensated) saccades. The earliest activation pulses, even those as short as 1.25 ms, elicited reacceleration >20 ms later. A similar effect can be produced by a brief inhibition of the feedback integrator in the model (Fig. 13).

Given that the onset of the ipsilateral activation reacceleration effect is similar to the time of contralateral compensatory reacceleration (Fig. 12), the ipsilateral OMV/CFN complex may be part of the feedback integrator. The mossy fiber projection from the paramedian pontine reticular formation (Yamada and Noda, 1987; Noda et al., 1990) suggests that the OMV/cFN complex receives an efference copy of the EBN motor command that could be appropriate for correcting the perturbations (Ohtsuka and Noda, 1992).

The left and right OMV are likely to contain the same cerebellar cortex microcircuits (Eccles, 1967). However, circuits on one side of the OMV apparently switch their role from a real-time feedforward controller during contraversive saccades to a feedback displacement integrator during ipsiversive saccades. As a feedforward controller, the OMV adjusts EBN and IBN activity to overcome the eye mechanics' sluggishness and prevent untimely OPN reactivation that would truncate saccades. As a displacement integrator, the circuits estimate the eye displacement and determine the deceleration time course. Neurons outside the cerebellar cortex may influence this switching role and may lie in a feedback loop that, with OMV P-cells, forms a neural integrator. A cerebellar nucleocortical loop (Houck and Person, 2015) seems unlikely to form the integrator because the sparse retrogradely labeled fastigial neurons did not overlap the high density of anterogradely labeled terminals from the OMV (Yamada and Noda, 1987). A more probable candidate is brainstem neurons that project directly or indirectly to the OMV as mossy fibers. If these neurons play this role, we predict that they should exhibit a gradual increase of activity just before and during a saccade like a long-lead burst neuron, and their activity should be different during contra- and ipsiversive saccades, e.g., have a directional tuning (Ohtsuka and Noda, 1992; Prsa et al., 2009). The involvement of long-lead burst neurons in a displacement integrator has been predicted previously (Scudder, 1988).

Comparison with cFN inactivation studies.

Activation near the midline of the vermis, which presumably inhibited both left and right cFNs, produced effects similar to those produced by bilateral cFN inactivation. The inactivation produced slight hypermetria of saccades in both directions, and the saccades were slower and had a prolonged deceleration phase (Robinson et al., 1993).

Both ipsilateral cFN inactivation and our brief ipsilateral P-cell activation produced hypermetria. In one study, ipsilateral cFN inactivation produced hypermetria consistent with our results, i.e., no change in the saccade acceleration phase and peak velocity but a prolonged saccade deceleration phase (Goffart et al., 2004). However, in an earlier study, saccade hypermetria occurred due to increased peak velocity and saccade duration (Robinson et al., 1993). The reason for this discrepancy is unclear.

Contralateral cFN inactivation slowed saccades and produced hypometria (Robinson et al., 1993; Goffart et al., 2004). Although our early brief P-cell activation also slowed saccades, the amplitudes were nearly normometric due to a compensatory reacceleration. We speculate that following contralateral cFN inactivation, the compensatory reacceleration from the intact ipsilateral cFN may be insufficient to fully compensate for the amplitude loss caused by slower saccades. In addition, the truncation of faster saccades causes them to be hypometric. This partial compensation may account for the smaller hypometric deficit of contraversive saccades after unilateral cFN inactivation (Iwamoto and Yoshida, 2002).

P-cell simple spike responses during saccades

What do our results mean for the roles of OMV P-cell simple spike (SS) activity in controlling saccades? Our results suggest that the SS activity of all OMV P-cells during both saccade acceleration and deceleration participate in determining the saccade trajectory. Population SS activity of contralateral P-cells, i.e., the cells that exhibit a pause in complex spikes (CSs) (CS-off error direction) after saccades under amplitude decrease adaptation

(Soetedjo and Fuchs, 2006; Soetedjo et al., 2008; Kojima et al., 2010), produce high firing rate during saccade acceleration and then pause during saccade deceleration (Herzfeld et al., 2015, their Fig. 4, green). This high firing rate is consistent with the lower firing rate of contralateral cFN neurons (Sun et al., 2016, their Fig. 7C). Our results regarding contralateral P-cell activation are consistent with the high gain of P-cell firing rate during acceleration to allow for fast and efficient compensation of the oculomotor mechanics, and the pause during deceleration prevents the activity from truncating the saccades via OPN re-activation.

The population SS activity of ipsilateral P-cells (CS-on direction) had a lower gain during saccade acceleration. Compared to the contralateral activity, it only reached about half of the peak activity, which was consistent with the higher firing rate of ipsilateral cFN neurons (Sun et al., 2016, their Fig. 7B). P-cell activity did not pause during saccade deceleration but instead lasted ~50 ms after the saccade ended (Herzfeld et al., 2015, their Fig. 4, brown). It is unclear whether this activity reflects the activity of a feedback displacement integrator, but the lingering activity is consistent with the passive discharge of a leaky integrator (Kustov and Robinson, 1995; Nichols and Sparks, 1995).

In conclusion, contralateral and ipsilateral OMV P-cells play distinct roles in controlling saccade trajectory. These roles align with a local negative feedback model of saccade generation. The contralateral OMV likely houses the feedforward inverse model of the oculomotor mechanics to estimate the appropriate saccade motor command, as evidenced by the low-latency deceleration effect on saccade trajectory and the compensatory reacceleration observed following perturbations. Conversely, the ipsilateral OMV, with its uncompensated long-latency reacceleration effect, is likely involved in the feedback forward model that predicts eye displacement. This prediction is likely accomplished by temporal integration of the efference copy of the saccade motor command. This conclusion would be strengthened by an

experiment that briefly inhibits P-cells and elicits contrasting effects—faster but normometric contraversive saccades and unchanged speed but hypometric ipsiversive saccades.

References:

Bahill AT, Clark MR, Stark L (1975) The main sequence, a tool for studying human eye movements. Mathematical Biosciences 24:191-204.

Barash S, Melikyan A, Sivakov A, Zhang M, Glickstein M, Thier P (1999) Saccadic dysmetria and adaptation after lesions of the cerebellar cortex. The Journal of neuroscience : the official journal of the Society for Neuroscience 19:10931-10939.

Barton EJ, Nelson JS, Gandhi NJ, Sparks DL (2003) Effects of partial lidocaine inactivation of the paramedian pontine reticular formation on saccades of macaques. Journal of neurophysiology 90:372-386.

Becker W, King, W.M., Fuchs, A.F., Jürgens, R., Johanson, G., Kornhuber, H.H. (1981) Accuracy of goal-directed saccades and mechanisms of error correction. In: Progress in Oculomotor Research (Fuchs AF, Becker, W., ed), pp 29-37. New York: Elsevier.

Collins CC, O'Meara D, Scott AB (1975) Muscle tension during unrestrained human eye movements. The Journal of physiology 245:351-369.

Eccles JC (1967) Circuits in the cerebellar control of movement. Proceedings of the National Academy of Sciences of the United States of America 58:336-343.

El-Shamayleh Y, Kojima Y, Soetedjo R, Horwitz GD (2017) Selective Optogenetic Control of Purkinje Cells in Monkey Cerebellum. Neuron 95:51-62.e54.

Fuchs AF (1967) Saccadic and smooth pursuit eye movements in the monkey. The Journal of physiology 191:609-631.

Fuchs AF, Luschei ES (1971) Development of isometric tension in simian extraocular muscle. The Journal of physiology 219:155-166.

Fuchs AF, Kaneko CR, Scudder CA (1985) Brainstem control of saccadic eye movements. Annual review of neuroscience 8:307-337.

Fuchs AF, Scudder CA, Kaneko CR (1988) Discharge patterns and recruitment order of identified motoneurons and internuclear neurons in the monkey abducens nucleus. Journal of neurophysiology 60:1874-1895.

Goffart L, Chen LL, Sparks DL (2004) Deficits in saccades and fixation during muscimol inactivation of the caudal fastigial nucleus in the rhesus monkey. Journal of neurophysiology 92:3351-3367.

Goldstein H, Robinson D (1984) A two-element oculomotor plant model resolves problems inherent in a single-element plant model. In: Soc Neurosci Abstr, p 909.

Harris CM, Wolpert DM (2006) The main sequence of saccades optimizes speed-accuracy trade-off. Biological cybernetics 95:21-29.

Herzfeld DJ, Kojima Y, Soetedjo R, Shadmehr R (2015) Encoding of action by the Purkinje cells of the cerebellum. Nature 526:439-442.

Houck BD, Person AL (2015) Cerebellar Premotor Output Neurons Collateralize to Innervate the Cerebellar Cortex. The Journal of comparative neurology 523:2254-2271.

Iwamoto Y, Yoshida K (2002) Saccadic dysmetria following inactivation of the primate fastigial oculomotor region. Neuroscience letters 325:211-215.

Iwamoto Y, Kaneko H, Yoshida K, Shimazu H (2009) Role of glycinergic inhibition in shaping activity of saccadic burst neurons. Journal of neurophysiology 101:3063-3074.

Judge SJ, Richmond BJ, Chu FC (1980) Implantation of magnetic search coils for measurement of eye position: an improved method. Vision research 20:535-538.

Jürgens R, Becker W, Kornhuber HH (1981) Natural and drug-induced variations of velocity and duration of human saccadic eye movements: evidence for a control of the neural pulse generator by local feedback. Biological cybernetics 39:87-96.

Kaneko CR (1997) Eye movement deficits after ibotenic acid lesions of the nucleus prepositus hypoglossi in monkeys. I. Saccades and fixation. Journal of neurophysiology 78:1753-1768.

Keller EL, Gandhi NJ, Shieh JM (1996) Endpoint accuracy in saccades interrupted by stimulation in the omnipause region in monkey. Visual neuroscience 13:1059-1067.

Kojima Y, Soetedjo R, Fuchs AF (2010) Changes in simple spike activity of some Purkinje cells in the oculomotor vermis during saccade adaptation are appropriate to participate in motor learning. The Journal of neuroscience : the official journal of the Society for Neuroscience 30:3715-3727.

Kojima Y, Ting JT, Soetedjo R, Gibson SD, Horwitz GD (2021) Injections of AAV Vectors for Optogenetics in Anesthetized and Awake Behaving Non-Human Primate Brain. Journal of visualized experiments : JoVE.

Kustov AA, Robinson DL (1995) Modified saccades evoked by stimulation of the macaque superior colliculus account for properties of the resettable integrator. Journal of neurophysiology 73:1724-1728.

Langer TP, Kaneko CR (1983) Efferent projections of the cat oculomotor reticular omnipause neuron region: an autoradiographic study. The Journal of comparative neurology 217:288-306.

Nichols MJ, Sparks DL (1995) Nonstationary properties of the saccadic system: new constraints on models of saccadic control. Journal of neurophysiology 73:431-435.

Noda H, Sugita S, Ikeda Y (1990) Afferent and efferent connections of the oculomotor region of the fastigial nucleus in the macaque monkey. The Journal of comparative neurology 302:330-348.

Ohtsuka K, Noda H (1992) Burst discharges of mossy fibers in the oculomotor vermis of macaque monkeys during saccadic eye movements. Neuroscience research 15:102-114.

Optican LM, Miles FA (1985) Visually induced adaptive changes in primate saccadic oculomotor control signals. Journal of neurophysiology 54:940-958.

Prsa M, Dash S, Catz N, Dicke PW, Thier P (2009) Characteristics of responses of Golgi cells and mossy fibers to eye saccades and saccadic adaptation recorded from the posterior vermis of the cerebellum. The Journal of neuroscience : the official journal of the Society for Neuroscience 29:250-262.

Quaia C, Lefevre P, Optican LM (1999) Model of the control of saccades by superior colliculus and cerebellum. Journal of neurophysiology 82:999-1018.

Robinson DA (1964) The mechanics of human saccadic eye movement. The Journal of physiology 174:245-264.

Robinson DA (1975) Oculomotor control signals. In: Basic mechanisms of ocular motility and their clinical implications (P. Bach-y-Rita GL, ed), pp 337-374. Oxford: Pergamon.

Robinson FR, Straube A, Fuchs AF (1993) Role of the caudal fastigial nucleus in saccade generation. II. Effects of muscimol inactivation. Journal of neurophysiology 70:1741-1758.

Sasaki S, Shimazu H (1981) Reticulovestibular organization participating in generation of horizontal fast eye movement. Annals of the New York Academy of Sciences 374:130-143.

Scudder CA (1988) A new local feedback model of the saccadic burst generator. Journal of neurophysiology 59:1455-1475.

Soetedjo R, Fuchs AF (2006) Complex spike activity of purkinje cells in the oculomotor vermis during behavioral adaptation of monkey saccades. The Journal of neuroscience : the official journal of the Society for Neuroscience 26:7741-7755.

Soetedjo R, Kojima Y (2022) Optogenetics in Complex Model Systems (Non-Human Primate). In: Measuring Cerebellar Function (Sillitoe RV, ed), pp 305-321. New York, NY: Springer US.

Soetedjo R, Kaneko CR, Fuchs AF (2002) Evidence that the superior colliculus participates in the feedback control of saccadic eye movements. Journal of neurophysiology 87:679-695.

Soetedjo R, Kojima Y, Fuchs AF (2008) Complex spike activity in the oculomotor vermis of the cerebellum: a vectorial error signal for saccade motor learning? Journal of neurophysiology 100:1949-1966.

Soetedjo R, Kojima Y, Fuchs AF (2019) How cerebellar motor learning keeps saccades accurate. Journal of neurophysiology 121:2153-2162.

Sparks D, Rohrer WH, Zhang Y (2000) The role of the superior colliculus in saccade initiation: a study of express saccades and the gap effect. Vision research 40:2763-2777.

Strassman A, Highstein SM, McCrea RA (1986a) Anatomy and physiology of saccadic burst neurons in the alert squirrel monkey. I. Excitatory burst neurons. The Journal of comparative neurology 249:337-357.

Strassman A, Highstein SM, McCrea RA (1986b) Anatomy and physiology of saccadic burst neurons in the alert squirrel monkey. II. Inhibitory burst neurons. The Journal of comparative neurology 249:358-380.

Strassman A, Evinger C, McCrea RA, Baker RG, Highstein SM (1987) Anatomy and physiology of intracellularly labelled omnipause neurons in the cat and squirrel monkey. Experimental brain research 67:436-440.

Sun Z, Junker M, Dicke PW, Thier P (2016) Individual neurons in the caudal fastigial oculomotor region convey information on both macro- and microsaccades. The European journal of neuroscience 44:2531-2542.

Sylvestre PA, Cullen KE (1999) Quantitative analysis of abducens neuron discharge dynamics during saccadic and slow eye movements. Journal of neurophysiology 82:2612-2632.

Takagi M, Zee DS, Tamargo RJ (1998) Effects of lesions of the oculomotor vermis on eye movements in primate: saccades. Journal of neurophysiology 80:1911-1931.

Takahashi M, Sugiuchi Y, Na J, Shinoda Y (2022) Brainstem Circuits Triggering Saccades and Fixation. The Journal of Neuroscience 42:789-803.

Taylor JR (1997) An introduction to error analysis : the study of uncertainties in physical measurements, 2nd ed Edition. [Place of publication not identified]: University Science.

Van Gisbergen JA, Robinson DA, Gielen S (1981) A quantitative analysis of generation of saccadic eye movements by burst neurons. Journal of neurophysiology 45:417-442.

Wilcox RR (2022) Chapter 5 - Comparing Two Groups. In: Introduction to Robust Estimation and Hypothesis Testing (Fifth Edition) (Wilcox RR, ed), pp 153-251: Academic Press.

Wolpert DM, Miall RC, Kawato M (1998) Internal models in the cerebellum. Trends in cognitive sciences 2:338-347.

Xu-Wilson M, Tian J, Shadmehr R, Zee DS (2011) TMS perturbs saccade trajectories and unmasks an internal feedback controller for saccades. The Journal of neuroscience : the official journal of the Society for Neuroscience 31:11537-11546.

Yamada J, Noda H (1987) Afferent and efferent connections of the oculomotor cerebellar vermis in the macaque monkey. The Journal of comparative neurology 265:224-241.

Yoshida K, Iwamoto Y, Chimoto S, Shimazu H (1999) Saccade-related inhibitory input to pontine omnipause neurons: an intracellular study in alert cats. Journal of neurophysiology 82:1198-1208.

Figure and Table Legends

Figure 1. A simplified block diagram of a local negative feedback model of the saccade generator. MN, motoneurons; EBN, excitatory burst neurons; DME, dynamic motor error.

Figure 2. The eye movement recording and the closed-loop systems used to deliver light pulses to the OMV. Left side shows the stepping target red dot on the screen and the scleral search coil. Middle shows normal eye position (green) and velocity (purple) time courses (dashed), and the effects of a light pulse (small blue bar, vertical line is light onset) on them. Right side shows triggering of laser light pulse by velocity signal.

Figure 3. Two exemplar un-normalized data sets from animal Sq (*A* and *B)* and Tm (*C* and *D*). Top to bottom: eye position, velocity, and acceleration panels. Red traces, control saccades; Blue traces, saccades perturbed by T0 light pulses (blue bars); error shades = 1SD. Vertical lines, detected time occurrence of activation effect at P=0.05 statistical difference between control and perturbed saccades. Number of trials: Sq, leftward control: 27, T0:16; rightward control: 22, T0: 22; Tm, leftward control: 34, T0: 33; rightward control: 42, T0: 27.

Figure 4. The effects of optical fiber location on saccade amplitude change. Sq, left column; Tm, right column. *A*, Saccade amplitude change vs. medio-lateral location of the optical fiber. Red circles, rightward saccades; black circles, leftward saccades. *B*, amplitude change in one saccade direction vs. the other. Filled circles, fiber located to the right (Sq) or to the left (Tm) of midline. *C*, actual locations of optical fibers of all experiments (green circles); injection sites (X). Other symbol represents a single experiment. The “d”s represent 6 experiments using variable

light pulse durations. +, an experiment that produced no significant change in saccade either saccade metrics or kinematics.

Figure 5. Population averages of *ipsiversive* saccade time courses. Traces are normalized (see Methods). *A* and *B*, animal Sq, T0, T10 and T20, T30, respectively. Top to bottom, eye position, velocity and acceleration panels. Horizontal bars, light pulses. Black, control saccades; red, T0 pulse perturbed saccades; green, T10 pulse perturbed saccades; blue, T20 pulse perturbed saccades; orange, T30 pulse perturbed saccades. Solid vertical lines in the corresponding colors indicate the P=0.05 difference from the control. *C* and *D*, animal Tm, same displays, conventions as in *A* and *B*.

Figure 6. Population averages of the effects of different light pulse duration on *ipsiversive* saccade amplitude. *A*, time courses of saccades after T0 and variable duration pulses. Horizontals bars, light pulses; pulse durations: red, 1.25 ms; green, 2.5 ms; black, 5 ms; brown, 10 ms. *B*, saccade amplitude vs. $\log_2$ of pulse durations (squares). Circles, control. Filled circle and squares, averages. Red lines, linear regression. N=328, 93, 120, 98 and 109 for control and pulse durations of 1.25, 2.5, 5 and 10 ms, respectively.

Figure 7. Population averages of *contraversive* saccade time courses. The same conventions as for Fig. 5. *A* and *B*, animal Sq. *C* and *D*, animal Tm.

Figure 8. Contraversive saccade duration vs. peak velocity after T0 and T10 pulses. *A* – *D*, T0 (red) and T10 (green) perturbed saccades in both Sq (A, C) and Tm (B, D), linear fits of data; control saccades (black). Histogram of saccade durations (right column), bin width = 2 ms.

Figure 9. Contraversive saccade deceleration duration vs peak velocity after T20 and T30 pulses. *A*, monkey Sq. T20 stimulation data, blue: perturbed saccades, black: control saccades. *B,* and *C*, monkey Tm. B, T20 stimulation data, blue; C, T30 stimulation data, brown; in both B and C, black are control saccades. Black lines are linear regressions; curved blue and orange lines are second-order polynomial fits. Histogram bin width = 2 ms.

Figure 10. Comparison of the effects of T20 and T30 stimulations on fast (*A* – *C*) and slow (*D* – *F*) contraversive saccades. *A* and *D*, monkey Sq, T20 stimulation data; fast saccades (A) 700–900 °/s; slow saccades (D) <600 °/s. *B* and *E*, monkey Tm, T20 stimulation data; fast saccades (B) 680–750 °/s; slow saccades (E) <500 °/s. *C* and *F*, monkey Tm, T30 stimulation data; fast saccades (C) 680–760 °/s; slow saccades (F) <496 °/s. Black, control; blue and brown, T20 and T30 stimulation data, respectively. Error shade = 1SD. Insets, saccade amplitude comparisons. Error bar = 1SD. Velocities of both animals were plotted in positive direction. Trials were selected to match the time course of saccade acceleration phase.

Figure 11. Population averages of saccade time courses resulting from stimulation of near midline OMV sites with mixed effects. The same organization and directional order as in Figs. 5 and 7. *A*, *B*, *E* and *F*, animal Sq. *A* and *B*, leftward saccades, N=50, 39, 46, 38, and 36 for control and T0, T10, T20 and T30, respectively. *E* and *F*, rightward saccades, N=35, 34, 34, 29,

and 26 for control, and T0, T10, T20 and T30, respectively. *C*, *D*, *G* and *H*, animal Tm. *C* and *D*, rightward saccades, N=84, 48, 43, 26, and 45 for control, and T0, T10, T20 and T30, respectively. *E* and *F*, leftward saccades, N=123, 87, 60, 78, and 66 for control, and T0, T10, T20 and T30, respectively.

Figure 12. Comparison of the timing of T0 ipsiversive reacceleration and T0 contraversive compensatory reacceleration. *A* and *B*, ipsiversive acceleration time courses of Sq and Tm, respectively. Red, control ipsiversive saccades; blue, T0 perturbed ipsiversive saccades. Error shades = 1SD. Solid vertical lines, mean time of occurrence of the ipsiversive reacceleration effect, dashed lines, 2SE. Red and blue data here are the same as black and red data in both Fig. 5A and C, respectively,. *C* and *D*, contraversive acceleration time courses of Sq and Tm, respectively. Red, control contraversive saccades; blue, T0 perturbed contraversive saccades. Error shades = 1SD. Solid vertical lines, mean time occurrence of contraversive compensatory reacceleration, dashed lines, 2SE. Red and blue data here are the same as black and red data in both Fig. 7A and C, respectively,

Figure 13. Model and simulations. *A*, The circuit of a local feedback model of the saccade generator. Abbreviations, DME, dynamic motor error; IBN, inhibitory burst neurons; OPN, omnipause neurons; EBN, excitatory burst neurons; MN, motoneurons. Equations and weight values, see Methods. Green pulse, contralateral P-cell activation inhibits EBN. Brown pulse, ipsilateral P-cell activation inhibits feedback integrator. *B*, Simulations of contralateral activation, top panel: position, lower panel, velocity. Black, control; red, early activation pulse; blue, later activation pulse. Bars, activation pulses. *C*, the same as in B, but with slower

saccades (*MaxEBNfr* = 750 spikes/s, see Material and Methods). *D*, Simulations of ipsilateral activation. E, Simulations of simultaneous ipsi- and contralateral activations.

Table 1. Summary of ipsiversive saccade metrics and optical activation timings.

Table 2. Summary of contraversive saccade metrics and optical activation timings.

Fig. 1

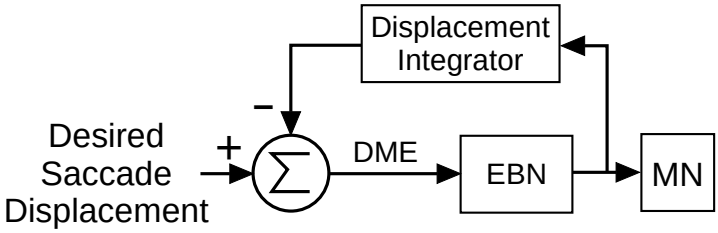
Displacement
Integrator
−
Desired
Saccade
Displacement
+
∑
DME
EBN
MN

Fig. 2

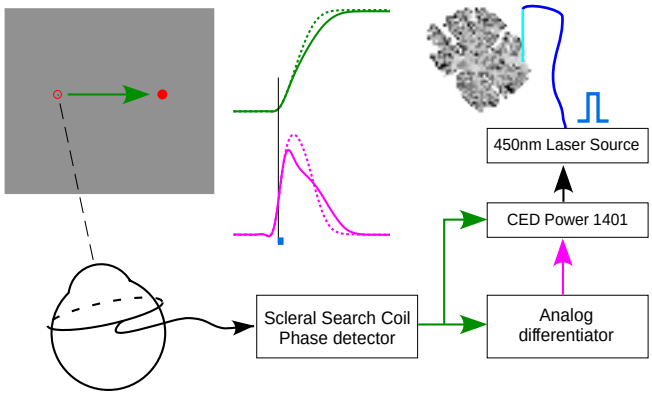
450nm Laser Source
CED Power 1401
Scleral Search Coil
Phase detector
Analog
differentiator

Fig. 3

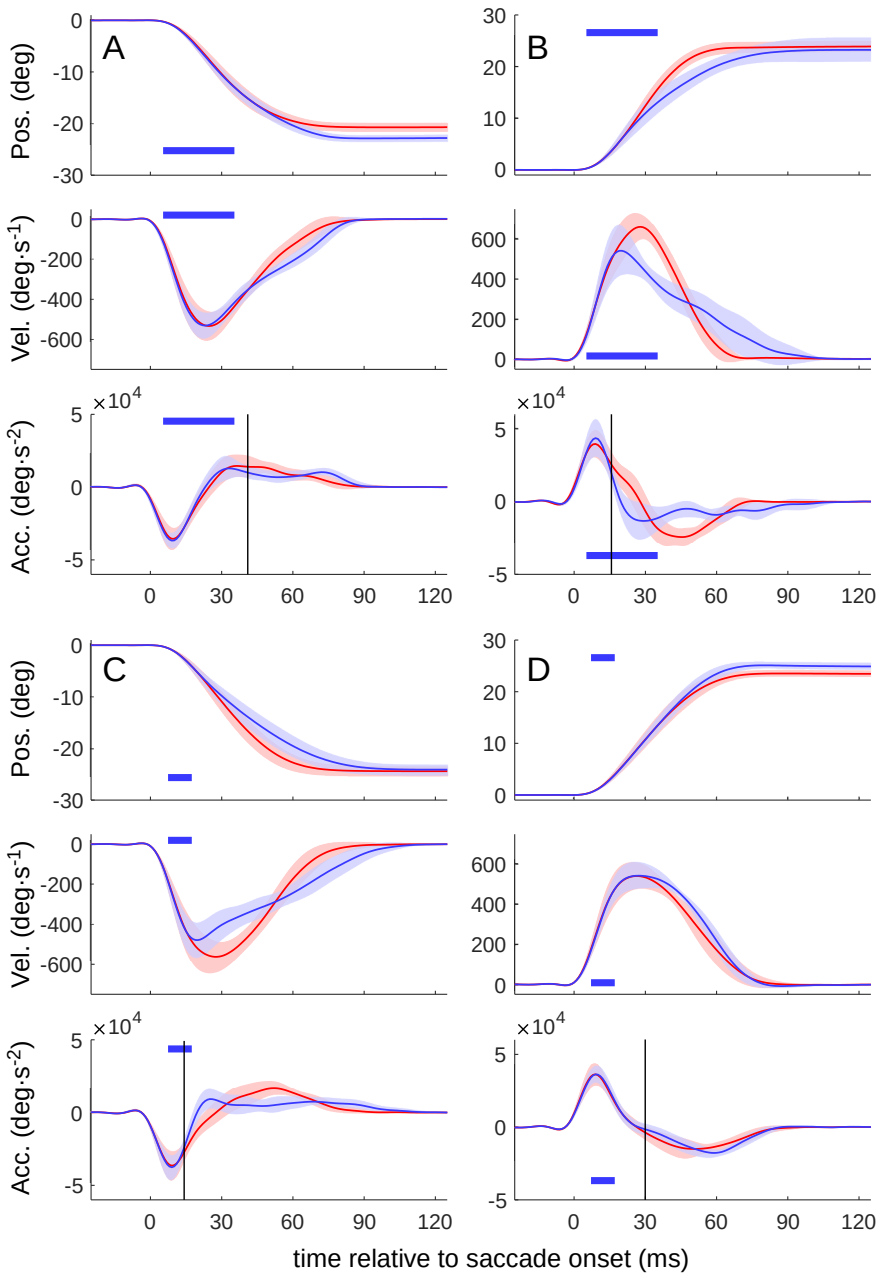
A
B
C
D
Pos. (deg)
Vel. (deg·s-1)
Acc. (deg·s-2)
×10^4
time relative to saccade onset (ms)

Fig. 4

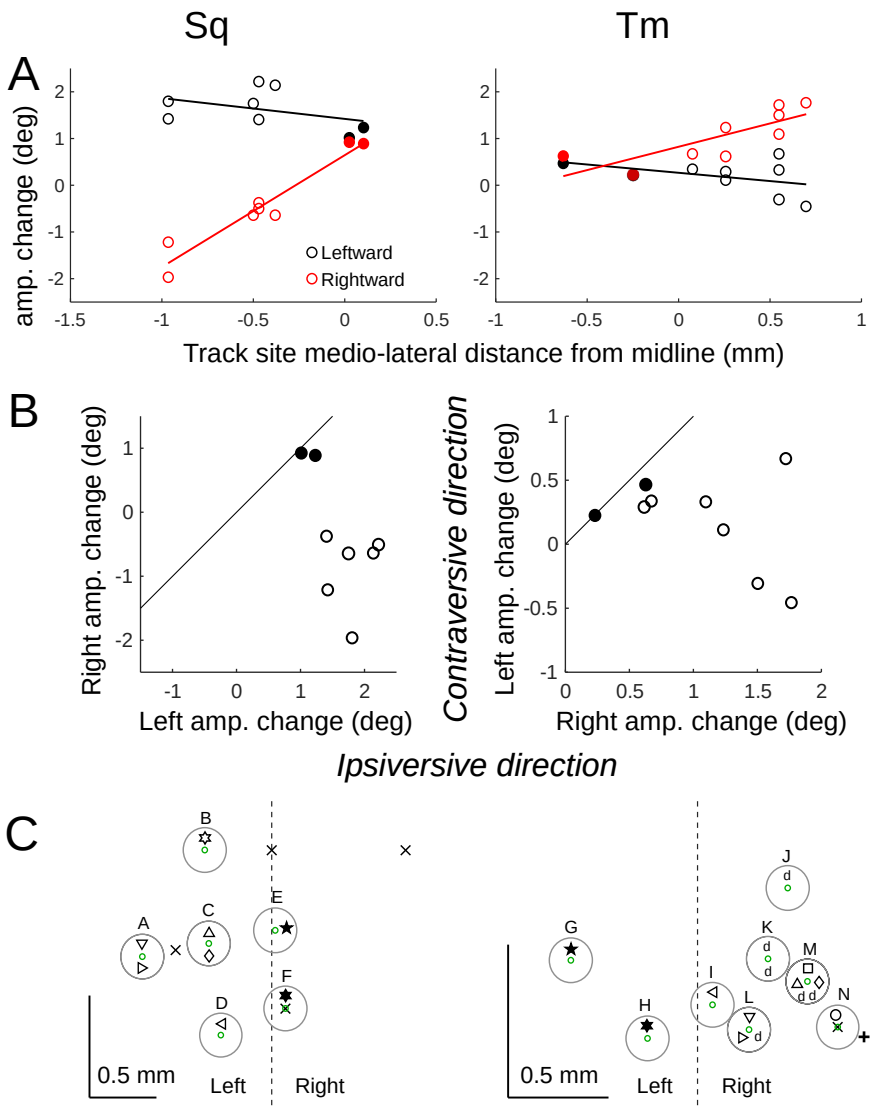
A
Sq
Tm
amp. change (deg)
Leftward
Rightward
Track site medio-lateral distance from midline (mm)
B
Right amp. change (deg)
Left amp. change (deg)
Contraversive direction
Left amp. change (deg)
Right amp. change (deg)
Ipsiversive direction
C
0.5 mm
Left
Right
0.5 mm
Left
Right

Fig. 5

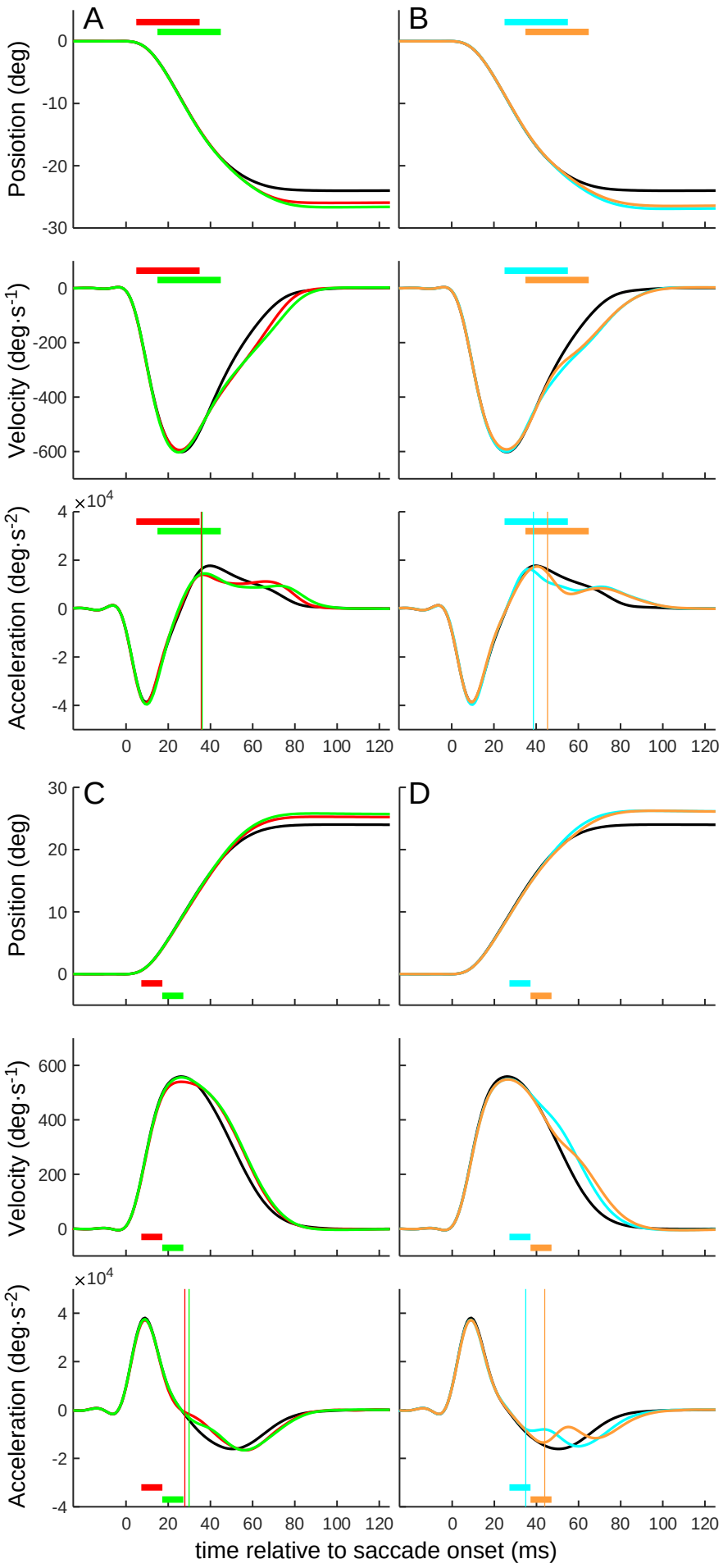
A
B
C
D
Posiotion (deg)
Velocity (deg·s-1)
Acceleration (deg·s-2)
Position (deg)
×10^4
time relative to saccade onset (ms)

Fig. 6

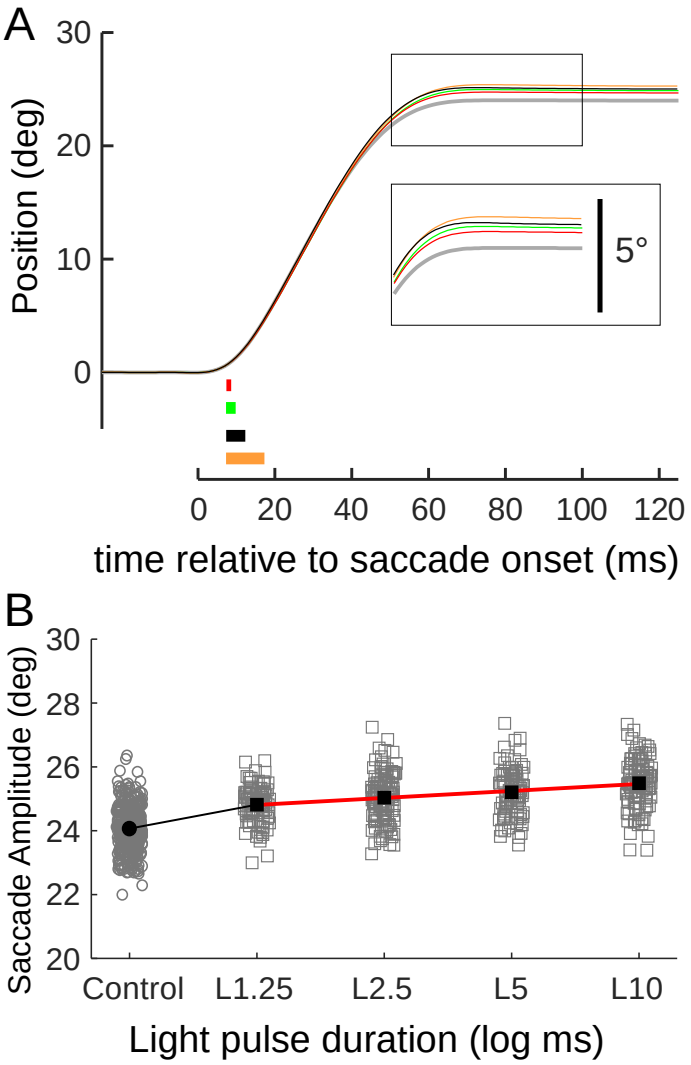
A
30
20
10
0
Position (deg)
5°
0
20
40
60
80
100
120
time relative to saccade onset (ms)
B
30
28
26
24
22
20
Saccade Amplitude (deg)
Control
L1.25
L2.5
L5
L10
Light pulse duration (log ms)

Fig. 7

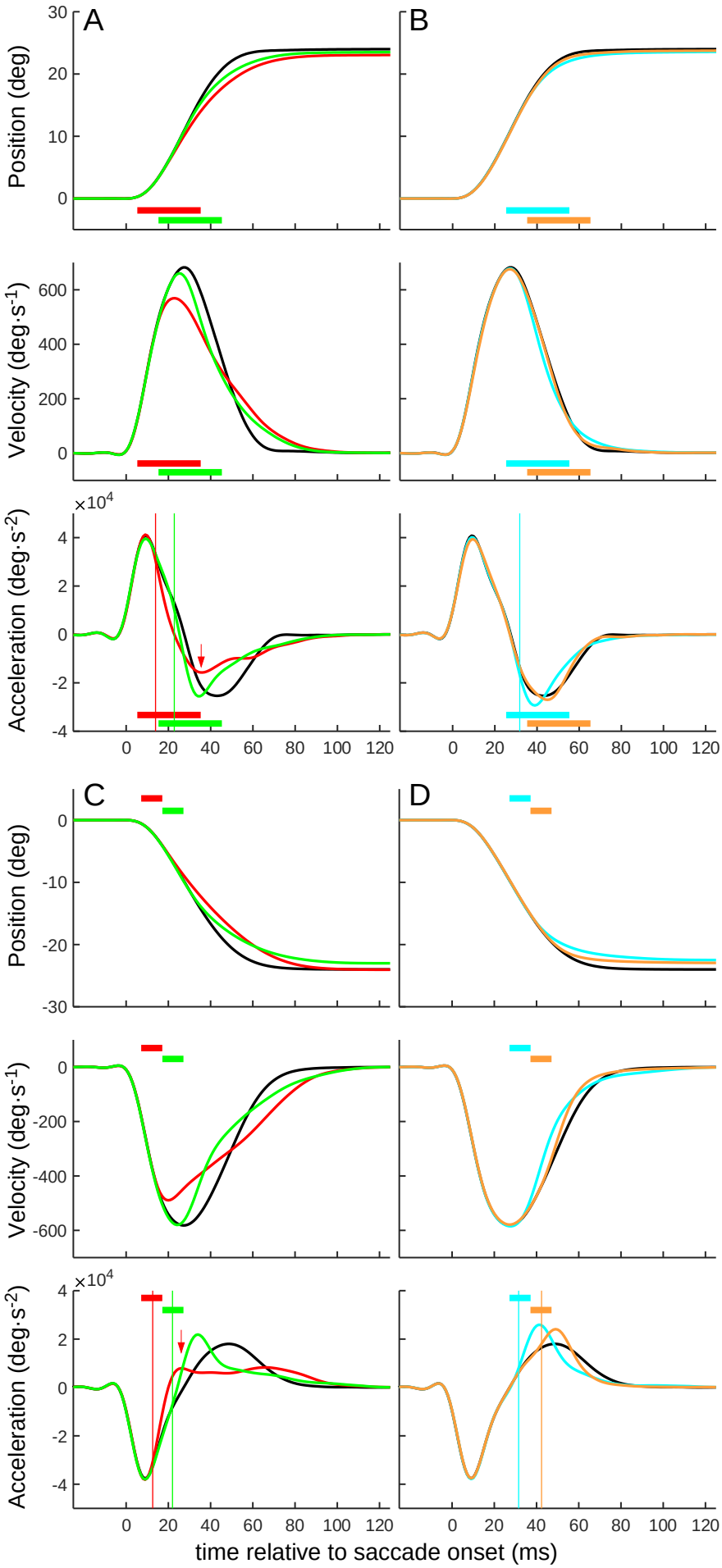
A
B
C
D
Position (deg)
Velocity (deg·s-1)
Acceleration (deg·s-2)
×10^4
time relative to saccade onset (ms)

Fig. 8

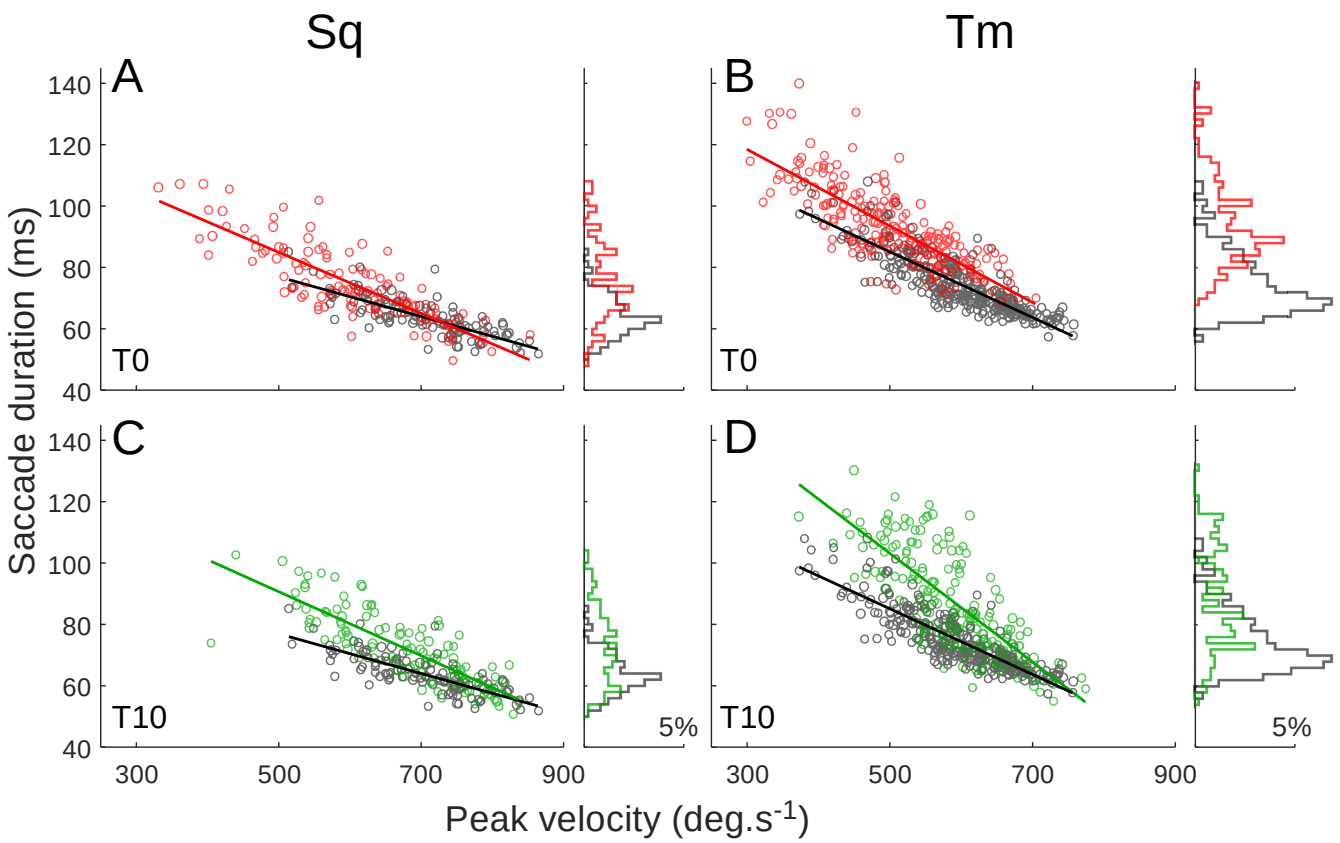
Sq
Tm
A
B
C
D
T0
T0
T10
T10
5%
5%
Saccade duration (ms)
Peak velocity (deg.s-1)
140
120
100
80
60
40
300
500
700
900

Fig. 9

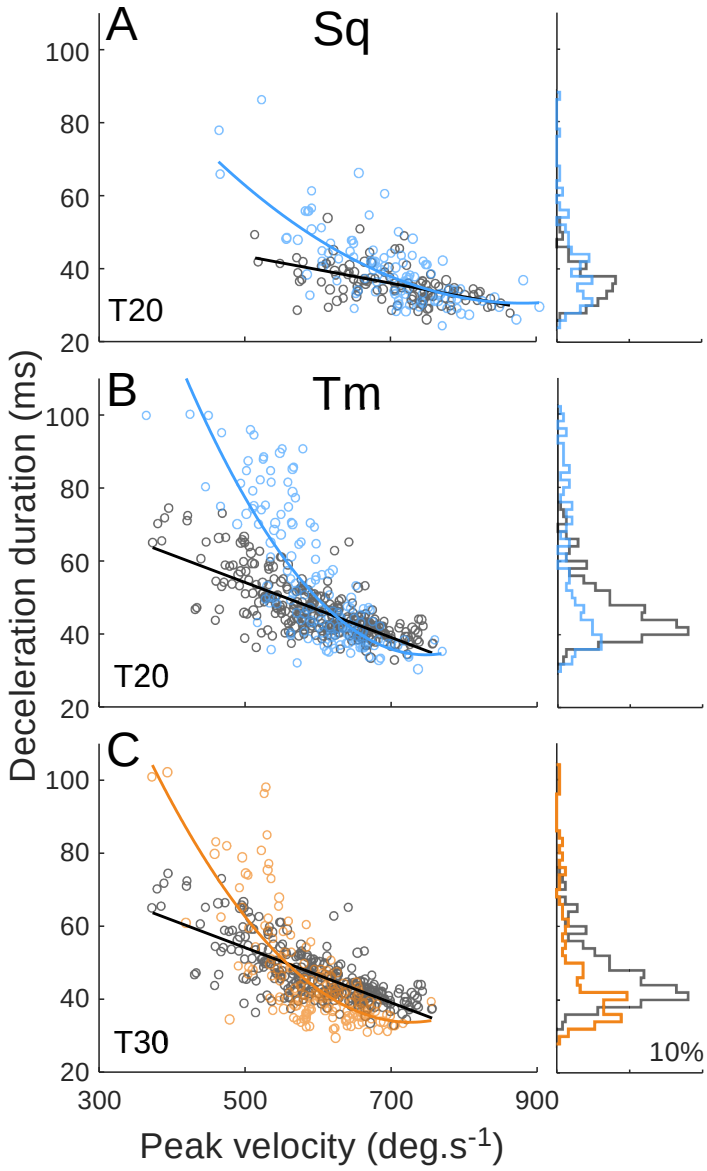
A
Sq
B
Tm
C
T20
T20
T30
10%
Deceleration duration (ms)
Peak velocity (deg.s-1)
100
80
60
40
20
300
500
700
900

Fig. 10

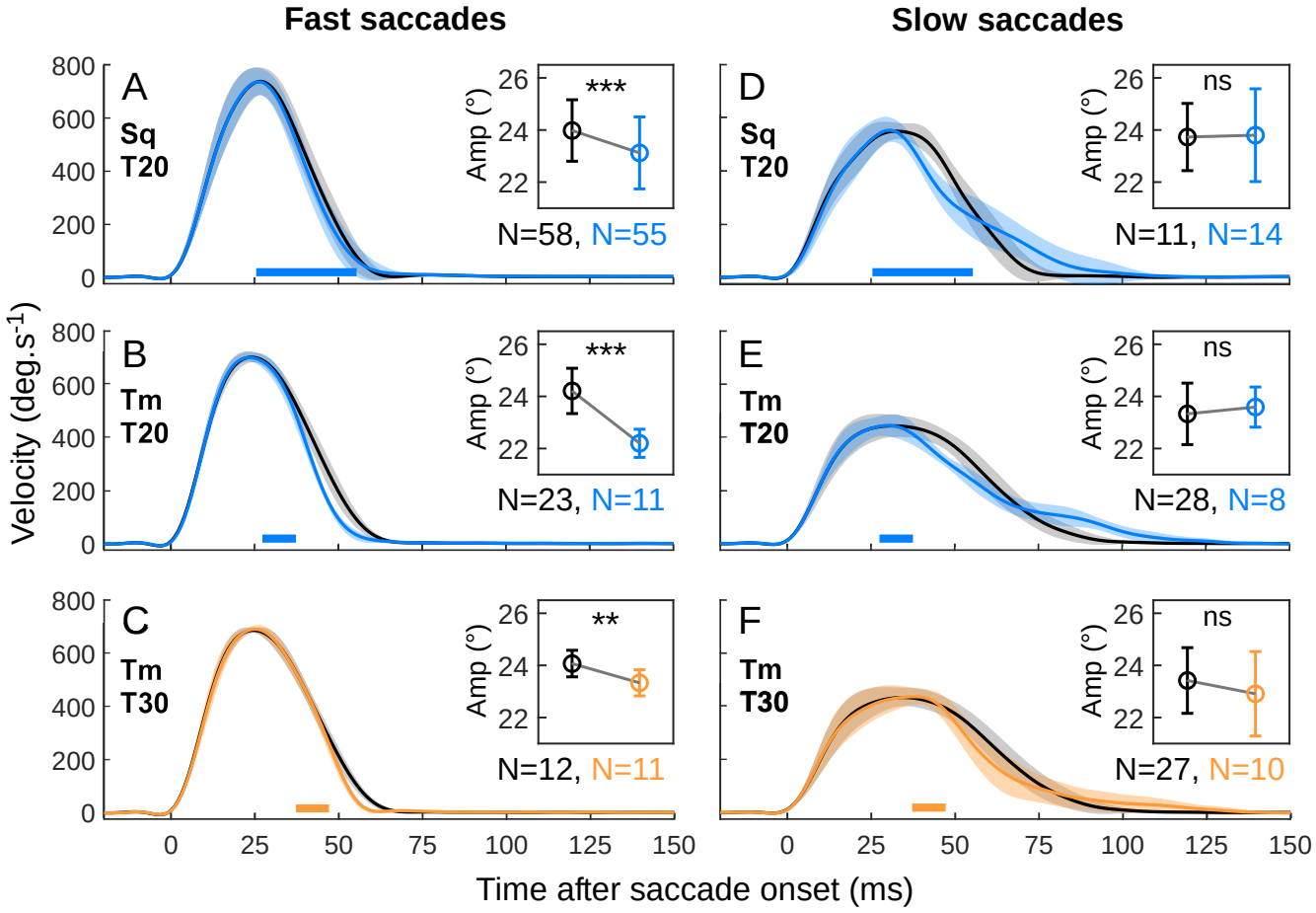
Fast saccades
Slow saccades
A
Sq
T20
B
Tm
T20
C
Tm
T30
D
Sq
T20
E
Tm
T20
F
Tm
T30
Amp (°)
***
**
ns
N=58, N=55
N=23, N=11
N=12, N=11
N=11, N=14
N=28, N=8
N=27, N=10
Velocity (deg.s-1)
Time after saccade onset (ms)

Fig. 11

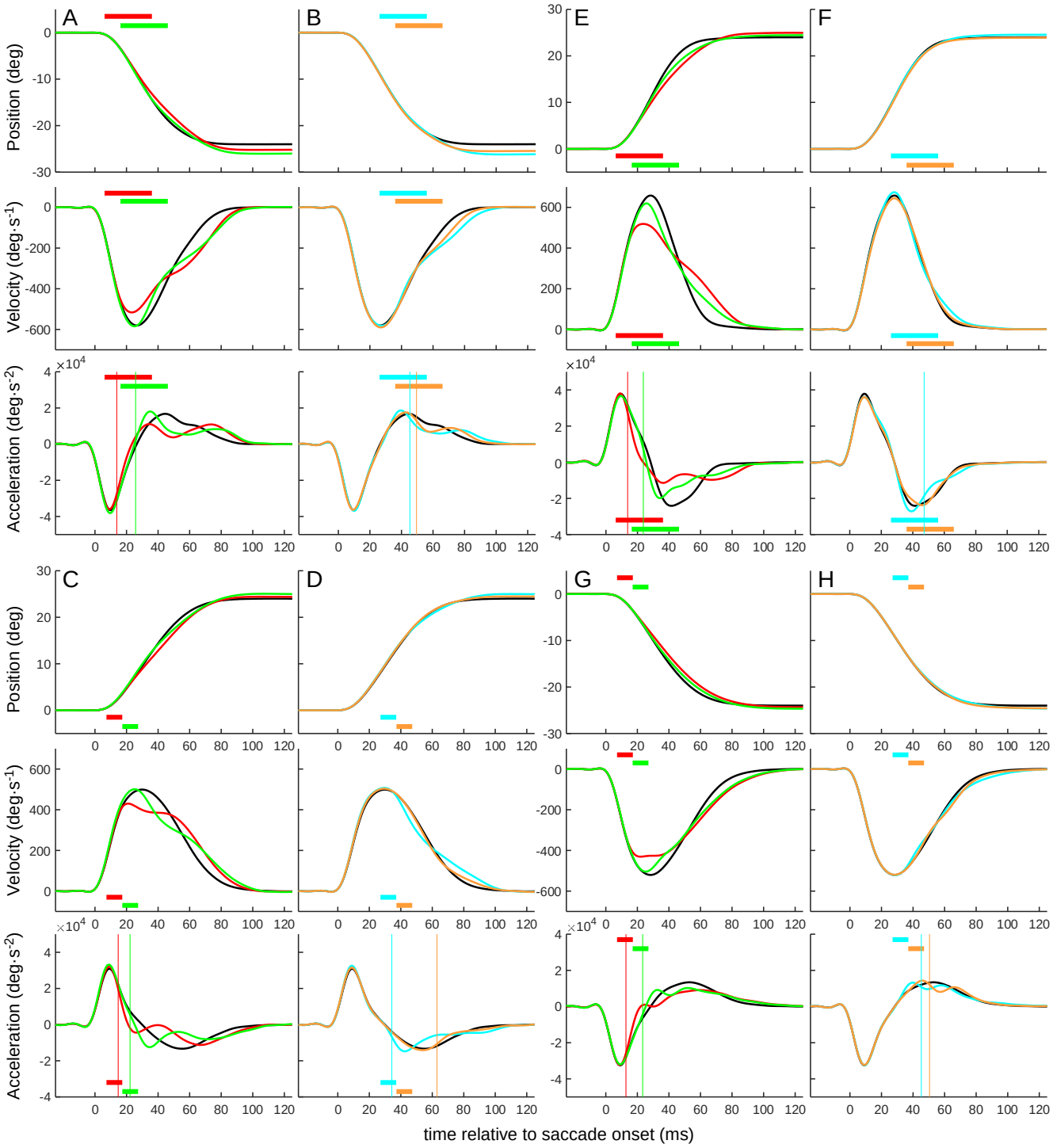
A
B
E
F
C
D
G
H
Position (deg)
Velocity (deg·s-1)
Acceleration (deg·s-2)
×10^4
time relative to saccade onset (ms)

Fig. 12

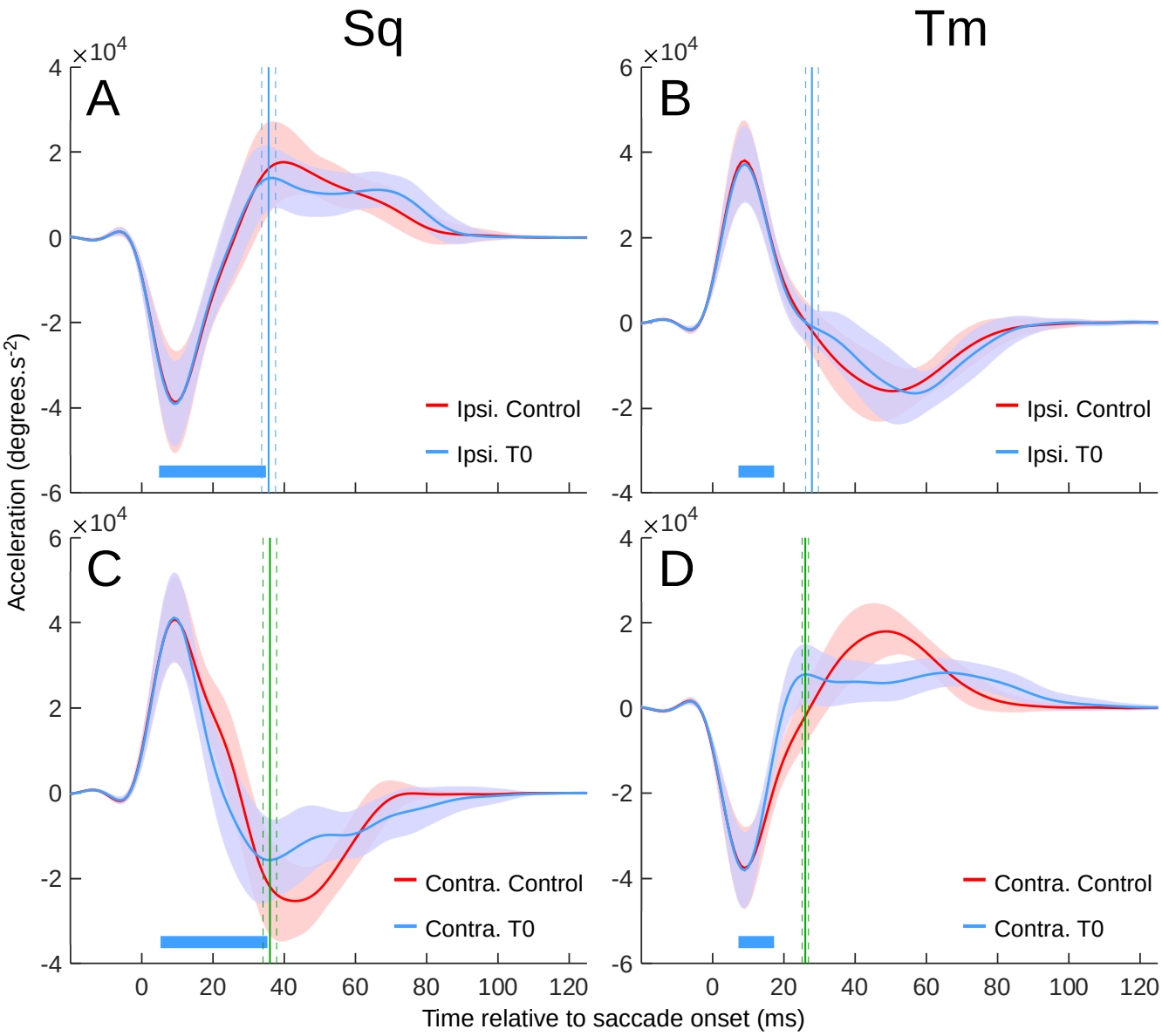
Sq
Tm
A
B
C
D
×10^4
Acceleration (degrees.s^-2)
Ipsi. Control
Ipsi. T0
Contra. Control
Contra. T0
Time relative to saccade onset (ms)

Fig. 13

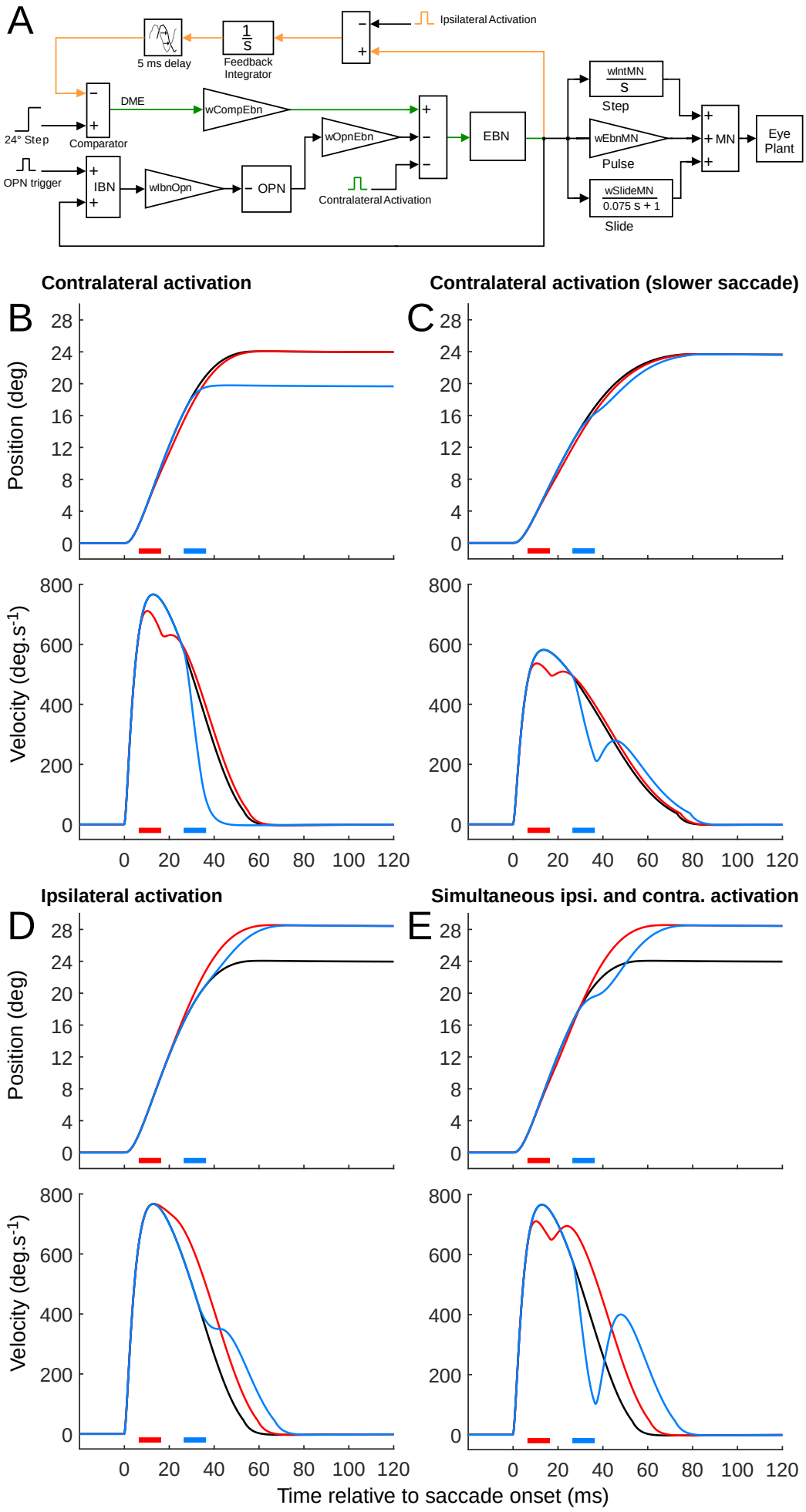
A
Ipsilateral Activation
5 ms delay
Feedback Integrator
DME
wCompEbn
24° Step
Comparator
OPN trigger
IBN
wIbnOpn
OPN
wOpnEbn
Contralateral Activation
EBN
wIntMN
Step
wEbnMN
Pulse
wSlideMN
0.075 s + 1
Slide
MN
Eye Plant
Contralateral activation
Contralateral activation (slower saccade)
B
C
Position (deg)
Velocity (deg.s-1)
Ipsilateral activation
Simultaneous ipsi. and contra. activation
D
E
Time relative to saccade onset (ms)

Table 1. Summary of ipsiversive saccade metrics and optical activation timings.

	Control	T0	T10	T20	T30
Animal Sq					
Number of Trials	181	130	138	150	150
Mean Pulse Onset (mean±1SD ms)		4.86±1.05	14.89±1.22	25.02±1.13	34.92±0.93
Reacceleration Effect Latency (mean±1SE ms)		30.76±0.97	21.27±1.17	13.61±0.71	10.36±1.18
Peak Velocity (mean±1SD º/s)	627.34±98.32	614.60±91.53	620.98±88.94	618.27±89.55	611.94±89.67
Saccade Amplitude (mean±1SD deg)	23.99±1.02	25.99±1.04	26.70±1.11	26.96±1.12	26.51±1.46
Acceleration Displacement (mean±1SD deg)	9.51±1.54	9.14±1.57	9.16±1.84	9.13±1.48	9.39±1.78
Deceleration Displacement (mean±1SD deg)	14.48±1.61	16.85±1.84	17.54±2.07	17.83±1.71	17.12±2.10
Animal Tm					
Number of Trials	295	222	212	226	249
Mean Pulse Onset (mean±1SD ms)		7.24±0.61	17.16±0.54	27.18±0.68	37.16±0.64
Reacceleration Effect Latency (mean±1SE ms)		20.66±0.89	12.53±1.18	6.88±3.28	6.43±2.39
Peak Velocity (mean±1SD º/s)	570.88±89.53	554.74±100.02	564.71±92.82	563.92±89.85	561.80±86.98
Saccade Amplitude (mean±1SD deg)	24.09±0.97	25.43±1.04	25.96±1.10	26.40±1.06	26.33±1.09
Acceleration Displacement (mean±1SD deg)	9.28±1.69	9.42±2.58	9.08±1.77	9.42±1.57	9.23±1.52
Deceleration Displacement (mean±1SD deg)	14.81±1.69	16.01±2.60	16.88±1.75	16.99±1.84	17.10±1.75

Table 2. Summary of contraversive saccade metrics and optical activation timings.

	Control	T0	T10	T20	T30
Animal Sq					
Number of Trials	111	114	115	103	99
Mean Pulse Onset (mean±1SD ms)		5.28±0.97	15.31±0.78	25.35±0.87	35.34±0.89
Deceleration Effect Latency (mean±1SE ms)		8.59±0.72	7.44±0.68	6.28±1.84	N/A
Peak Velocity (mean±1SD, º/s)	703.36±76.29	596.75±105.59	675.32±94.24	696.85±81.60	698.88±75.92
Saccade Amplitude (mean±1SD deg)	23.81±1.13	22.88±1.87	23.32±1.74	23.34±1.46	23.57±1.35
Acceleration Displacement (mean±1SD deg)	11.11±1.49	8.03±2.01	9.50±1.37	10.66±1.25	10.86±1.39
Deceleration Displacement (mean±1SD deg)	12.70±1.56	14.85±2.82	13.82±2.42	12.68±1.76	12.71±1.52
Animal Tm					
Number of Trials	288	214	170	153	167
Mean Pulse Onset (mean±1SD ms)		7.13±0.79	17.16±0.63	27.19±0.66	37.11±0.73
Deceleration Effect Latency (mean±1SE ms)		5.31±0.53	4.94±0.42	4.21±0.66	5.18±0.68
Peak Velocity (mean±1SD, º/s)	597.68±77.67	500.25±83.81	584.85±71.95	595.73±67.13	592.47±63.49
Saccade Amplitude (mean±1SD deg)	23.96±1.04	24.04±1.19	22.99±1.66	22.42±1.45	22.86±1.02
Acceleration Displacement (mean±1SD deg)	9.83±1.54	6.05±1.54	8.13±1.03	9.72±1.39	9.71±1.39
Deceleration Displacement (mean±1SD deg)	14.13±1.63	17.99±1.82	14.86±2.23	12.71±2.05	13.15±1.61